CHALMERS
UNIVERSITY OF TECHNOLOGY

On The Modelling of Jet Grouting For Deep Excavation Analysis

Assessing the Suitability of Shotcrete Material Model for Field Applications

Master's thesis in Civil Engineering

David Tran
Yohanes Armediaz

DEPARTMENT OF ARCHITECTURE AND CIVIL ENGINEERING
CHALMERS UNIVERSITY OF TECHNOLOGY
Gothenburg, Sweden 2021
www.chalmers.se

Master's thesis 2021

On The Modelling of Jet Grouting For Deep Excavation Analysis

Assessing the Suitability of Shotcrete Material Model for Field Applications

DAVID TRAN
YOHANES ARMEDIAZ

CHALMERS
UNIVERSITY OF TECHNOLOGY

Department of Architecture and Civil Engineering
Division of Geology and Geotechnics
Chalmers University of Technology
Gothenburg, Sweden 2021

On The Modelling of Jet Grouting For Deep Excavation Analysis
Assessing the Suitability of Shotcrete Material Model for Field Applications
DAVID TRAN
YOHANES ARMEDIAZ

Supervisor : Carl Jonsson, Keller Grundläggning AB
Supervisor : Sinem Bozkurt, Department of Architecture and Civil Engineering
Examiner: Minna Karstunen, Department of Architecture and Civil Engineering

Master's thesis 2021
Department of Architecture and Civil Engineering
Division of Geology and Geotechnics
Chalmers University of Technology
SE-412 96 Gothenburg
Telephone +46 31 772 1000

Cover: Image of jet grout retaining columns in the studied excavation site in Oslo, Norway (Keller, 2021).

Typeset in LaTeX
Printed by Chalmers Reproservice
Gothenburg, Sweden 2021

On The Modelling of Jet Grouting For Deep Excavation Analysis
Assessing the Suitability of Shotcrete Material Model for Field Applications
DAVID TRAN, YOHANES ARMEDIAZ
Master's thesis 2021
Masters Programme Infrastructure and Environmental Engineering
Department of Architecture and Civil Engineering
Chalmers University of Technology

Abstract

Retaining wall is a common solution to secure excavations and to minimise surrounding ground settlements, jet grouting is implemented. Currently, jet grouting structures are commonly numerically modelled with Mohr-Coulomb model which is a linear elastic and perfectly plastic model. However, in actuality, jet grouting behaves non-linearly. An alternative approach is to utilize a new novel material model, Shotcrete, originally created for tunnel linings. However, utilising Shotcrete for jet grouted retaining walls had rarely been done and not much research has been conducted. In this thesis, the two material models for a jet grouted retaining columns were compared. The practicality of Shotcrete model in the industry is also explored. The study is based on an actual excavation project in Oslo, Norway. Model parameters were derived from the original geotechnical investigation, new laboratory tests and literature values. The results show that both models predict similar deformations. The similarity can be explained by the fact that the columns are still in the elastic region, where Shotcrete model adopts Mohr-Coulomb failure criteria similar to Mohr-Coulomb model. Additionally, deformations can be caused by other factors in the system, which are the same in the two models. Furthermore, combination of the original geotechnical investigation and additional laboratory tests were insufficient to derive the necessary model parameters for the model. Instead, literature values were used which may not be suitable for jet grouting materials. In conclusion, the study have shown that there is not enough merit to implement Shotcrete model over Mohr-Coulomb model.

Keywords: material model, Mohr-Coulomb, jet grouting, retaining wall, Shotcrete, Plaxis 2D, deep excavation

Acknowledgements

Firstly, we would like to take the opportunity to thank Chalmers University of Technology for giving us the opportunity to grow our competence through the Master's programme and perform the research as part of our Master's thesis.

We would also like to thank our supervisors and examiner, Minna Karstunen and Sinem Bozkurt, for their support and advice throughout the thesis. Without their guidance and consistent help, this research would not have been possible. We are extremely grateful for the assistance.

To the staffs of Keller, especially Robert Thurner and our supervisor, Carl Jonsson, thank you for providing the research project and the assistance particularly on the practical aspect. We really appreciate it that we are given the chance to visit one of your actual construction site, allowing us to further learn about the work that you do, especially on the jet grout material.

We would like to express our gratitude to our friends and opposition partner, Behrang Alikhanzadeh Alamdari and Simon Larsson, for going through the process together with us, supporting and helping each other. Doing the project alongside you guys gave made the project much more enjoyable.

Diaz: Last, but not least, I would like to thank my partner, Gan Tze Li, for her continuous support and understanding. You have always had my back and I would not be where I am right now without you behind my back.

David Tran, Gothenburg, June 2021
Yohanes Armediaz, Gothenburg, June 2021

Contents

List of Figures

List of Tables

List of Symbols

Latin letters

p	Deviatoric stress
q	Mean stress
E_{28}	Young's modulus after 28 days
E_{oed}^{ref}	Odeometer stiffnes
$f_{c,28}$	Uniaxial compressive strength after 28 days
$f_{t,28}$	Uniaxial tensile strength after 28 days
f_{c0n}	Normalized initial yeild stress in compression
f_{cfn}	Normalized failure strength
f_{cun}	Normalised residual strength
$G_{c,28}$	Fracture energy in tension after 28 days
E_1/E_{28}	Time dependency of elastic stiffness
$f_{c,1}/f_{c,28}$	Ratio of uniaxial compressive strength after 1 day and 28 days
t_{50}^{cr}	Time at 50% of creep
t_{50}^{shr}	Final shrinkage strain
t_{50}^{shr}	Time at 50% of shrinkage
$s_{u,ref}$	Undrained shear strength
m	power of stress level dependancy
c	cohesion

Greek letters

ν	Poisson's ratio
ψ	Angel of dilantancy
σ_1'	Major stress
σ_2'	Minor stress
σ_3'	Minor stress
ϵ_{cp}^p	Plastic peak strain in uniaxial compression at age 1h,8h and 24 h
ϕ^{cr}	Ratio of creep vs elastic strain
ϵ_∞^{shr}	Final shrinkage strain
γ_{unsat}	Unsaturated Unit weight
γ_{sat}	Saturated Unit weight
$\lambda*$	Modified compression index
$\kappa*$	Modified swelling index

1
Introduction

1.1 Motivation

Due to rapid population growth in recent years, there is an increasing pressure to densify urban areas. With that, there is an increase in demand for crucial infrastructure to continue supporting the area such as accommodation, transportation and utilities. Nevertheless, some cities including Oslo are underlain by soft soils (e.g. Eide et al., 1972). This can make underground construction works in the cities challenging.

One approach to tackle the issue is via ground improvement. Jet grouting is a well-recognised ground improvement method (Croce et al., 2014). Developed in Japan in the 1970s, jet grouting improves soil by increasing the strength and decrease the permeability (Nakanishi, 1974). This helps the soil to withstand forces that it would not have withstand otherwise. Its usage has grown in popularity due to its flexibility from deep braced excavations (Zhang et al., 2021), tunnel supports (Ochmański et al., 2015) and foundation reinforcement (Modoni and Bzówka, 2012).

In the industry, complex geotechnical designs are often carried out based on numerical analysis. One of the most popular methods used is the Finite Element Method (FEM). FEM is a method of numerical analysis which approximates continuous element using a finite representation. The approximated solutions are solved by differential equations which describe the physical problem. For geotechnical problems, PLAXIS 2D is one of the most used software to apply FEM.

Currently, jet grout material is commonly modelled in PLAXIS using the Mohr-Coulomb material model, which assumes a linear elastic and perfectly elastic behaviour (PLAXIS, 2019). However, similar to concrete, this material model is unable to accurately predict jet grouts behaviour near failure, where cracks are expected to appear, which results in softening of the material. As a result, the Mohr-Coulomb material model may lead to overestimation of the strength and underestimation of the displacement of the jet grouts in the model, which can be catastrophic.

A novel material model that could be used to predict the behaviour of jet grouts is be the Shotcrete model. The model was developed in 2014 in Graz for sprayed concrete application in tunnelling (Schädlich and Schweiger, 2014). One of the features of the model which makes it appropriate for modelling jet grouts is the consideration

of strain softening. This is important for concrete-like materials such as jet grouts which develop cracks prior to failure.

The validity of Shotcrete material model on the stress analysis has been tested in the case of sprayed concrete (Saurer et al., 2014) and reinforced concrete (Maatkamp et al., 2016). However, not much research has been done the suitability of using Shotcrete material model for deformation analysis for jet grouts in deep excavations. Furthermore, model parameters required for the model may not be commonly requested in the industry. This may lead the price and time taken during the design stage to increase. Thus, this thesis is intended to investigate the suitability of the model.

1.2 Aim & Objectives

The aim of this thesis is to assess the suitability of the Shotcrete material model for modelling a jet grouted retaining wall for deep excavation analysis in the industry.

Primarily, investigation on whether there is any difference in the simulation results, specifically the deformations, from Shotcrete material model and the traditional Mohr-Coulomb model will be performed. This is performed by creating two identical numerical models with different material models for jet grouting material based on an actual construction site in one of the Scandinavian countries. The results from the two models will then be compared against each other.

Additionally, the practicality of Shotcrete material model will be researched. The model is expected to require model parameters that are uncommon in the industry. Thus, the additional effort to obtain the parameters will be examined.

1.3 Limitations

In reality, the study site to be used in this thesis is a complex project, consisting of different types of retaining structures. Therefore, several assumptions were made to create a simplified model for the purposes of this thesis. Furthermore, due to time constraints, there is a need to delimit the scope of the study. Due to these reasons, the following main limitations are identified:

- Since the analysis is made in PLAXIS 2D, plane strain analysis is assumed. Neither corner effects nor effects from uneven soil profile in and out of plane direction is considered.

- According to the original geotechnical investigation provided, prior to the commencement of this study, boreholes were only conducted within the excavation of the study site. No information is available for the soil profile in the active side of the excavation. This study assumes the soil profile to be the same as

that found in the jet grout columns.

- Whilst there are existing buildings in the vicinity, these are assumed to be founded on piles up to the bedrock level. Thus, they are assumed to not affect the study site and are therefore excluded in the model.

- Time-dependency feature of the Shotcrete model is not explored in this study.

A discussion on how the limitations can affect this study will be provided in a later chapter.

1.4 Organisation of thesis

The organisation of the thesis will be as follows:

- Chapter 1 - Introduction
  The general background and current issues has been described. The objectives and the scope have also been established.

- Chapter 2 - Background
  The background on jet grouting and the theory of constitutive modelling in geotechnical engineering will be discussed. This includes the two material models to be adopted to model jet grouting in this study.

- Chapter 3 - Methodology & Setup
  A description of the methodology and setup used for this thesis will be presented.

- Chapter 4 - Results & Discussions
  Outputs from the model will be presented here. The differences between the two models, and the practicality of the Shotcrete model will be discussed.

- Chapter 5 - Conclusions & Recommendations
  A summary of the thesis will be presented, alongside with recommendations for further research.

2
Background

This chapter sets out to outline what is currently known about jet grouting and how it can affect the outcome of this thesis. Additionally, the theory behind constitutive modelling for soft soils and jet grouting will be discussed, including the material models that will be used in this thesis and how they are derived.

2.1 Background on Jet Grouting

The process of jet grouting is accomplished through a jet grouting string. The string consist of jointed rods with conduits which provide fluids to the monitor, attached at the end of the string. The monitor transforms the pressure in the string into jet streams. The jet grouting process is initiated by drilling to the desired depth. This is conducted by a drill bit mounted on the monitor. Then, the jetting is performed trough the nozzles on the monitor. The jetting causes soil to erode as a result of the high pressure and increases the pore-water pressure. The high pressure also affects the soil and the injected fluids to rise to surface between the the string and the borehole wall. This results in a mix of soil and grout fluid called the spoil. Spoil is an by-product of the process, minimizing the amount of spoil leads to better cost-efficiency.

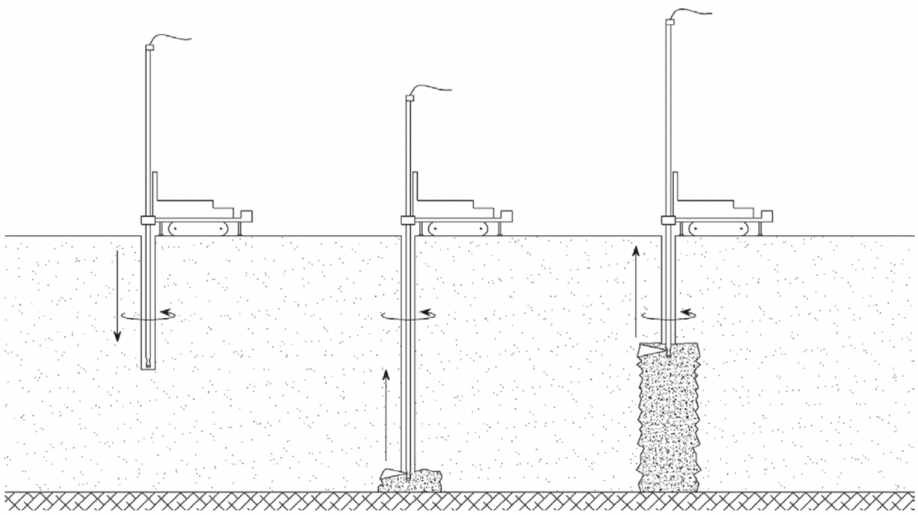

Figure 2.1: Typical Jet Grouting Procedure (Croce et al., 2014)

At present, three jet grouting techniques exist, single, double and triple fluid, referring to the number of fluids that are injected. In single fluid, only grout is injected into the system. The cementation and the erosion is done by the grout in this case. Further, in the double fluid system, a coaxial jet of air is added to assist in remoulding the soil. The jet of air is placed around the grouting nozzle. The air jet assist the erosion of of the soil, hence increasing the eroding distance. Water is another medium that can be used instead of air, however, this is a less common method. The triple fluid system inject three different fluids air, water and grout. In this case, the nozzles are separated into erosion and grouting process. Water and air is jetted to initiate the erosion process in the upper part of of the monitor. Compared to the other techniques, the grout emerges in a lower velocity since the soil already is eroded.

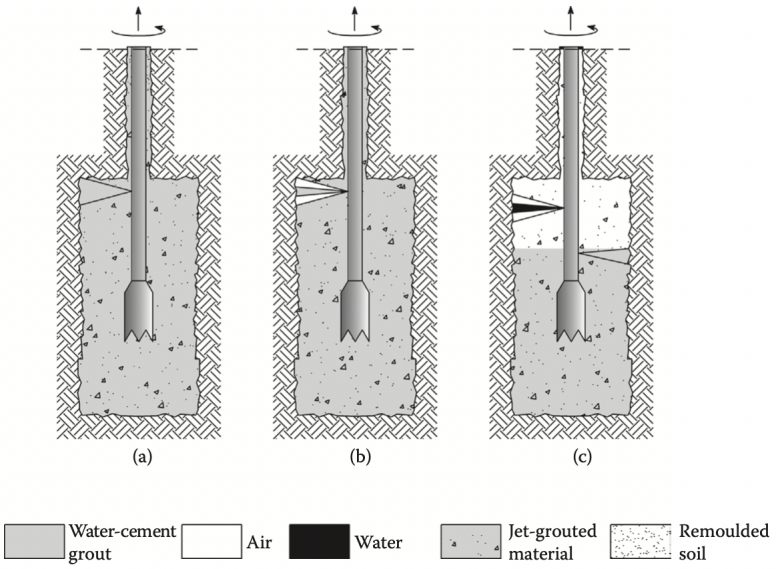

Figure 2.2: Three jet grouting techniques: (a) single fluid, (b) double fluid and (c) triple fluid (Croce et al., 2014)

Much research has been conducted on jet grouting. The theoretical modelling of the mechanical phenomena for single fluid technique is well-known, where it functions differently depending on the cohesiveness of the soil (Modoni et al., 2006). Its characteristic strength has also been investigated (Toraldo et al., 2018). Additionally, the properties of jet grouts are highly dependent on the construction (e.g. Zhang et al., 2021). This finding may affect the analysis of the two models when compared to actual deformation as the models are unable to capture the effect of construction.

Based on literature reviews, jet grouting is most commonly modelled using the Mohr-Coulomb model (e.g. Zhang et al., 2021, Feng, 2009, Bredy, Jandora, et al., 2019). The model is able to provide sufficiently accurate analysis of the geotechnical problems, at least when considering the ultimate limit state.

2.2 Application of Jet Grouting in Excavation

Excavation is one of the most common problems in geotechnical engineering. Extreme caution needs to be taken when excavation is carried out in dense, urban areas. A major concern with excavations in urban areas is the impact of the ground movements on adjacent buildings, caused by ground movements from the excavation process. In the worst case scenario, it can lead to collapse of the excavation and destroy adjacent structure, e.g Nicoll Highway collapse in Singapore (Whittle and Davies, 2006). Therefore, excavation has to be carefully executed. However, no matter how careful the the excavation is designed, the excavation will still result in ground movements (Clough, 1990). A solution to the problem at hand is to utilize soil improvement techniques to minimize the ground movements to an acceptable level. The definition of the acceptable level varies depending on region, type of projects and foundations, but commonly the lateral displacement at the top of the wall is limited to 0.3% of the depth of the wall (Long, 2001, Lazarte et al., 2015).

Currently, ground improvement techniques are popular solutions for construction problems. New techniques, materials and application are regularly proposed within ground improvement sector. As such, jet grouting technique has become one of the more successful ground improvement techniques in the market. Compared to traditional techniques such as sheet piles, jet grouting can achieve larger columns of cemented material by drilling smaller holes into the ground while minimizing disturbance in the surrounding soil. Also, columns can be formed to continuous elements to form different shapes and sizes with low permeability and good strength properties. Consequently, jet grouting has offered new solutions to geotechnical problems (Croce et al., 2014. Furthermore, jet grouting can be performed in difficult settings, where there is limited space or spaces that is difficult to reach. Thus jet grouting is a good technique to utilize for strengthening existing structures.

2.3 Constitutive Modelling

2.3.1 Modelling Based on Numerical Analysis

Due to the complexity of soil behaviour (both soil-soil and soil-structure interaction), there is a need to simplify the system in order to estimate deformations mathematically. To achieve this, several constitutive models are utilised (Karstunen and Amavasai, 2017). In geotechnical analysis, the most common type of constitutive modelling is elasto-plastic modelling. The figure below shows four existing constitutive models that are commonly used for modelling, three of which are elasto-plastic models.

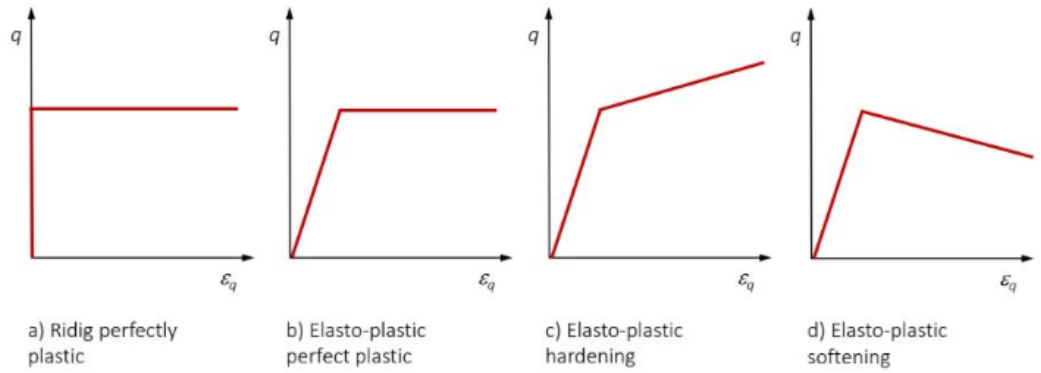

Figure 2.3: Four commonly used constitutive models (Karstunen and Amavasai, 2017)

The rigid perfectly plastic model assumes that the soil does not deform at all until failure occurs (Karstunen and Amavasai, 2017). This model is commonly used for ultimate limit state analyses, such as the calculation of slope stability . The elasto-plastic perfectly plastic model, of which the most well-known is the Mohr-Coulomb model, deviates slightly from the previous model by having a linear elastic behaviour that is based on Hooke's law. This model is commonly used as a first approximation of soil behaviour (PLAXIS, 2019). Increasing the complexity further, the elasto-plastic hardening and elasto-plastic softening models differs from the first two models in the plastic range, where the deviatoric stress increases and decreases accordingly with respect to the strain of the material. The latter two models are more appropriate to be used to model soft clays which can be either normally consolidated (NC) or overly consolidated (OC). Soft clay tends to exhibit strain hardening or softening depending on the stress state and stress history. For jet grouting, the elasto-plastic perfectly plastic model is the one that is most commonly used.

Elasto-plastic models are based on theory of plasticity where four criteria are required. The first one is the elastic law. This law governs the relationship between the effective stress state of the material and the elastic strain. This relationship can either be linear (e.g Hooke's law) or non-linear. Additionally, this relationship can also be both stress- and time-dependent. For the models used in this thesis, both linear and non-linear relationship will be adopted. Stress-dependency will also be observed in most of the models. Nevertheless, while time-dependency is available for one of the models used, it will not be utilised in this thesis.

The yielding criterion is defined next to delimit the elastic region. In the 1-D space, it is called a yield stress, whereas in the 2-D or 3-D space, it is called a yield function or yield surface. The yield function is commonly defined as f and is expressed using effective stresses or (effective) stress invariants. For geotechnical analysis, p' (the mean effective stress) and q (deviator stress) are the two stress invariants that are commonly used. Therefore, the yield surface is expressed as follows:

$$f(\sigma'_{ij}) = 0 \quad \Rightarrow \quad f(p', q) = 0 \tag{2.1}$$

To determine the direction of the plastic flow, i.e the proportion of the strain increments, a rule is required. For a purely elastic material, this rule is provided by the Poisson's ratio ν' which determines the incremental strains for all the stress invariants of the material. A similar rule is required for the plastic region, which is called the flow rule.

To do this, plastic potential g is introduced, where:

$$g(\sigma'_{ij}, \zeta) = 0 \quad \Rightarrow \quad g(p', q, \zeta) = 0 \tag{2.2}$$

In the above equation, ζ defines the size of the plastic potential. Once the plastic potential is defined, the flow rule can then be defined as:

$$d\varepsilon^p_p = d\lambda \frac{\partial g}{\partial \sigma_p} \quad ; \quad d\varepsilon^p_q = d\lambda \frac{\partial g}{\partial \sigma_q} \tag{2.3}$$

In general, the plastic multiplier $d\lambda$ controls the magnitude of the plastic strain increments, while $\frac{\partial g}{\partial \sigma_{ij}}$ controls the direction of the plastic flow.

The yield function f and the plastic potential g are generally different functions. In the event that they are the same, an associated flow is assumed, where the direction of the plastic flow is perpendicular to the yield surface. Otherwise, a non-associated flow is assumed. The latter is often assumed for models that adopt a Mohr-Coulomb failure criterion, which is the standard for the models that are used in this thesis.

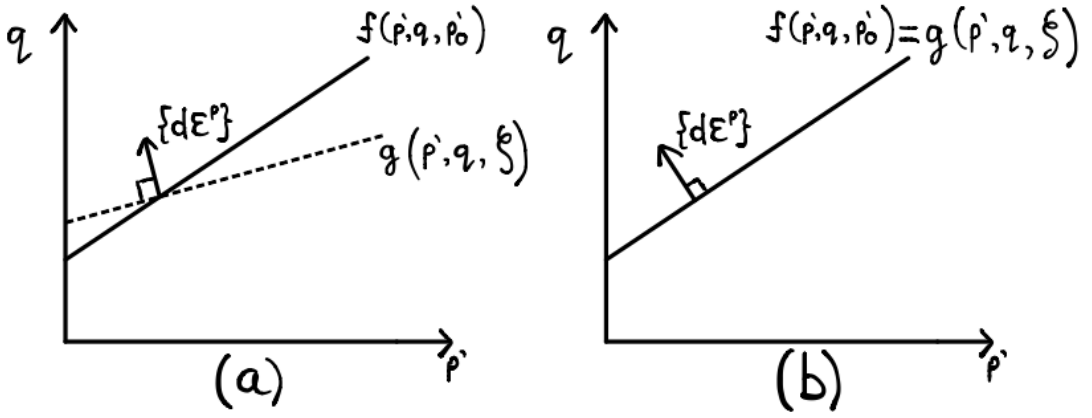

Figure 2.4: (a)Non-associated and (b) Associated Flow Rule

Lastly, a hardening rule is required. This rule determines how the yield surface evolves during yielding. This is done by adding a hardening parameter h into the yield function. In geotechnical analysis, the hardening parameter is commonly taken to be the apparent pre-consolidation pressure p'_0. This makes equation (2.1) to evolve into:

$$f(\sigma'_{ij}, h) = 0 \quad \Rightarrow \quad f(p', q, p'_0) = 0 \tag{2.4}$$

Consequently, the hardening rule is then defined as:

$$p_0' = p_0'(\varepsilon_p^p, \varepsilon_q^p) \quad ; \quad dp_0' = \frac{\partial p_0'}{\partial \varepsilon_p^p} d\varepsilon_p^p + \frac{\partial p_0'}{\partial \varepsilon_q^p} d\varepsilon_q^p \tag{2.5}$$

Equation (2.5) shows that the hardening parameter p_0' is a function of the plastic strain. This will consequently affect yield function based on equation (2.4) as the yield function f is a function of p_0'. Depending on the models, the yield function can either expand or shrink in the p'-q stress space. Alternatively, the model can also remain unaffected by hardening rule, rendering the hardening parameter h unnecessary. This phenomena can be observed in perfectly plastic models. Furthermore, models may assume only deviatoric or volumetric hardening only, instead of the double-hardening assumed in the general case above.

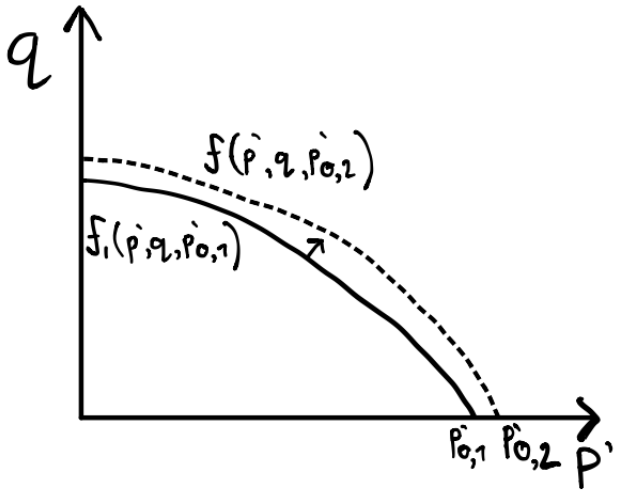

Figure 2.5: Hardening Rule Example

2.3.2 Models for Jet Grouting

In this thesis, two material models will be used to model the behaviour of the jet grouting material. They are Mohr-Coulomb and Shotcrete model. The theory behind the two models will be described below, including their respective advantages and disadvantages.

2.3.2.1 Mohr-Coulomb Model

The Mohr-Coulomb (MC) model is a simple linear elastic-perfectly plastic model. The linear elastic part of the model is based on Hooke's law for isotropic materials, while the perfectly plastic part is based on Mohr-Coulomb failure criterion.

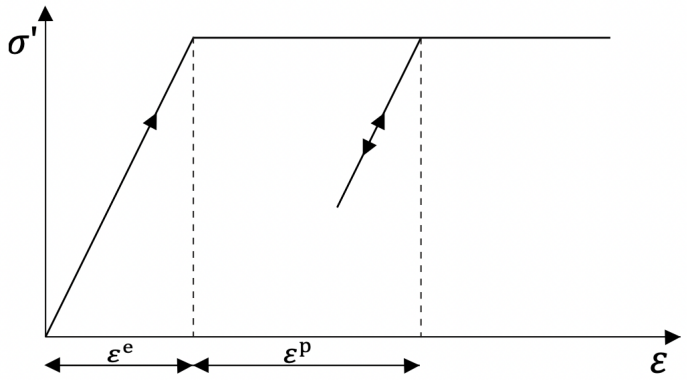

Figure 2.6: Fundamental of linear elastic perfectly plastic model (PLAXIS, 2019)

MC model adopts Hooke's law for its elastic law given as follows:

$$\sigma^e = \mathbf{D}^e \varepsilon^e \tag{2.6}$$

In equation (2.6) above, $\mathbf{D}^e$ is the elastic stiffness matrix, which governs the incremental strains in the elastic region based on the material's Poisson's ratio ν' and effective Young's modulus E' (note both are in terms of effective stresses).

In the MC model, yielding takes place when the shear stress τ in any plane is equal to the shear strength τ_f of the material.

$$\tau = \tau_f = c' + \sigma' tan\phi' \quad \Rightarrow \quad f(\sigma_i') = \tau - \sigma_i' tan\phi' - c' = 0 \tag{2.7}$$

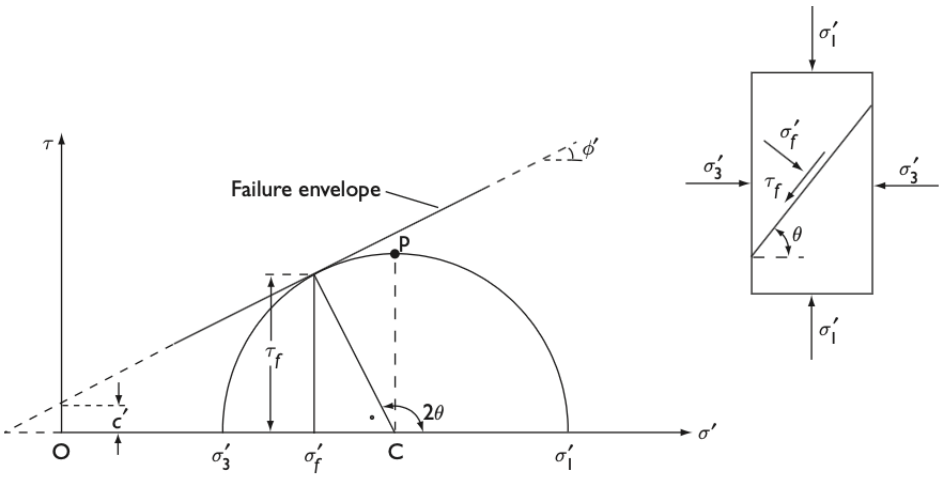

Figure 2.7: Mohr-Coulomb Failure Criterion (Craig, 2004)

where c' and ϕ' are strength parameters, cohesion intercepts and friction angle which are material properties that are unique to a particular soil. This means that these values need to be determined, instead of assigned. In the principal (effective) stress

space, the yield surface of the MC model is an irregular hexagon (see Figure 2.9).

Equation (2.7) can also be re-written in terms of p' and q as follows:

$$f(p', q) = q - \eta p' - c^* = 0 \quad ; \quad \eta = \frac{6sin\phi'}{3 - sin\phi'} \quad , \quad c^* = \frac{6ccos\phi'}{3 - sin\phi'} \tag{2.8}$$

The MC model assumes a non-associated flow rule, thus a plastic potential needs to be defined. This is performed by introducing the dilatancy angle ψ'. Thus, the plastic potential function is defined as:

$$g(\sigma_i') = \tau - \sigma_i' tan\psi' - const. = 0 \quad , \quad \psi' < \phi' \tag{2.9}$$

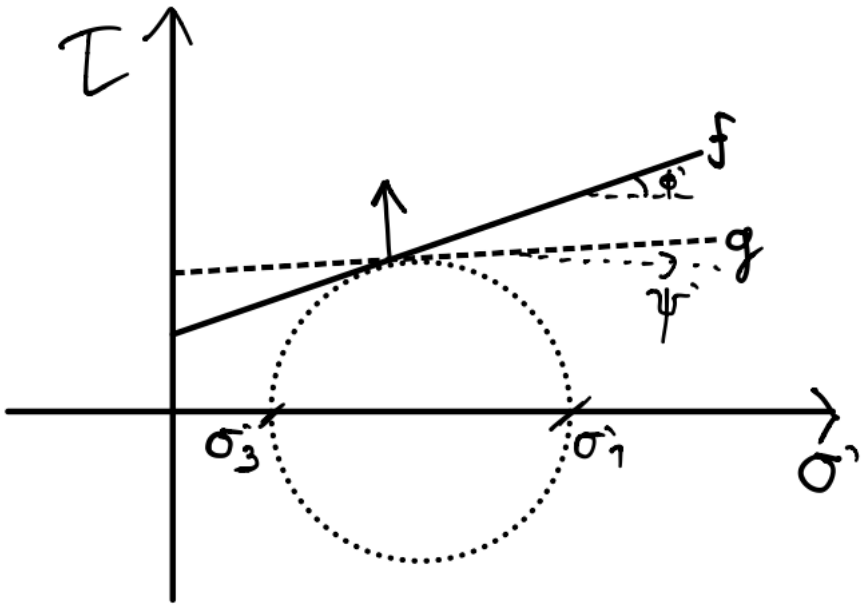

Figure 2.8: MC Plastic Potential Function

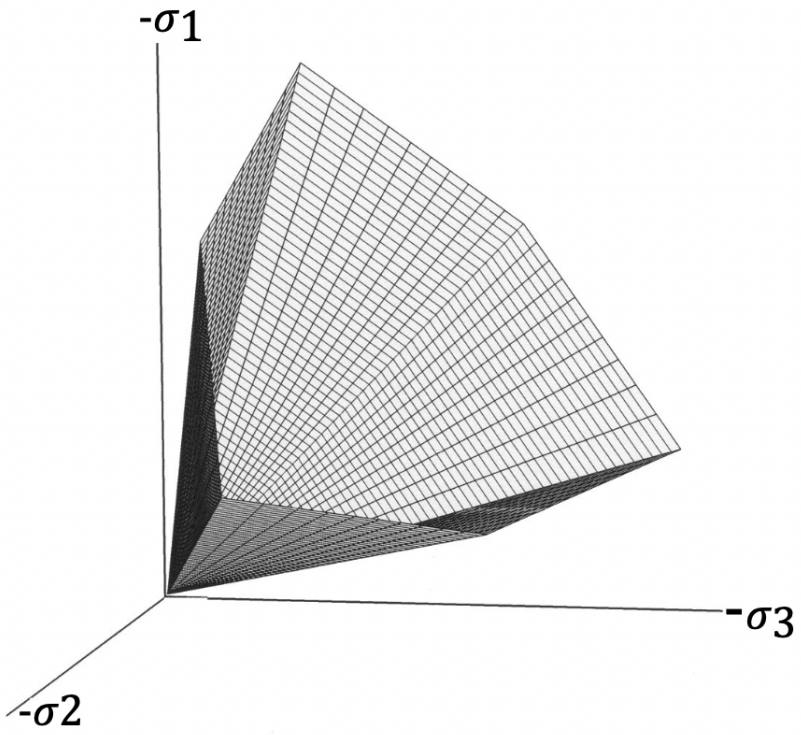

Figure 2.9: MC model yield surface in the principal stress space (tension is +ve, c'=0) (PLAXIS, 2019)

Some geomaterials tend to dilate when sheared, especially for denser materials such as dense sand and OC clays (Reynolds, 1885). This results in an increase in volume. Conversely, looser materials such as loose sand or soft clay contract. When translated in the horizontal plane, the mobilised friction angle can be larger than then internal friction angle sliding on the plane. This difference is taken into account by the dilatancy angle.

Since the MC model assumes perfectly plastic, no hardening rule is applied to the model.

Table 2.1 below shows the model parameters that will be required as an input when running the analysis.

Table 2.1: Parameters of Mohr-Coulomb

Name	Unit	Comment
Stiffness parameters		
E'	GPa	Effective Young's modulus
ν'	-	Poisson's ratio
Strength parameters		
c'	kPa	Effective cohesion
ϕ'	°	Effective friction angle
ψ	°	Angle of dilatancy

While the MC model has been commonly used to model jet grouting materials, it is actually unable to correctly predict the behaviour of the material. This is because jet grouting materials behaves similarly to concrete, where there is an onset of cracks as the material is reaching the yield surface (Waichita et al., 2020). In this sense, the model will over-predict the strength near yielding as the model assumes that the material is linearly elastic until yielding. Therefore, to model the material more accurately, a better constitutive that can take into account the cracks will be required.

2.3.2.2 Shotcrete Model

In reality, jet grouts behaves non-linearly. An alternative model to be considered is the Shotcrete material model by Schädlich and Schweiger, 2014. In PLAXIS, the model is named "Concrete". The model takes into account the non-linear and time-dependent behavior of concrete. The model was originally proposed for modelling sprayed concrete used as tunnel lining. Recently, further application of Shotcrete has been utilized, especially for cement treated soil (Schweiger et al., 2014).

In Table 2.2 an overview of the model parameters for Shotcrete is given. The total strain is determined by elastic, plastic, creep and shrinkage strains. However, the time-dependent stiffness and strength parameters are not taken into account in this thesis. Thus, shrinkage and creep were neglected since it was not considered necessary for the site considered in the thesis.

$$\varepsilon = \varepsilon^e + \varepsilon^p + \varepsilon^{cr} + \varepsilon^{shr} \tag{2.10}$$

Table 2.2: Parameters of Shotcrete

Name	Unit	Comment
Stiffness parameters		
E_{28}	GPa	Young's modulus after 28 days
υ	-	Poisson's ratio
Strength parameters		
$f_{c,28}$	MPa	Uniaxial compressive strength after 28 days
$f_{t,28}$	MPa	Uniaxial tensile strength after 28 days
ψ	°	Angle of dilatancy
f_{c0n}	-	Normalized initial yield stress in compression
f_{cfn}	-	Normalized failure strength
f_{cun}	-	Normalized residual strength
ε_{cp}^{p}	-	Plastic peak strain in uniaxial compression at age 1h, 8h and 24 h
$G_{c,28}$	kN/m	Fracture energy in compression after 28 d
f_{tun}	-	Normalized residual tensile strength
$G_{t,28}$	kN/m	Fracture energy in tension after 28 d
Time-dependent parameters		
E_1/ E_{28}	-	Ratio of Young's modulus after 1 day and 28 days
$f_{c,1}/f_{c,28}$	-	Ratio of f_c after 1 day and 28 days
φ^{cr}	-	Ratio of creep vs elastic strains
t_{50}^{cr}	-	Time at 50% of creep
$\varepsilon_{\infty}^{shr}$	-	Final shrinkage strain
t_{50}^{shr}	-	Time at 50% of shrinkage

The model uses Mohr-Coulomb yield surface for compression loading, combined with a Rankine yield surface in tensile stress range, Figure 2.10, where f_{cy} and f_t are the uniaxial compressive and tensile yield strengths, respectively. The yield functions are defined as:

$$F_c = \frac{\sigma_1 - \sigma_2}{2} + \frac{\sigma_1 + \sigma_3 - 2 * \sigma_{rot}}{2} * \frac{f_{cy}}{2 * \sigma_{rot} + f_{cy}} \tag{2.11}$$

$$F_t = \sigma_1 - f_t \tag{2.12}$$

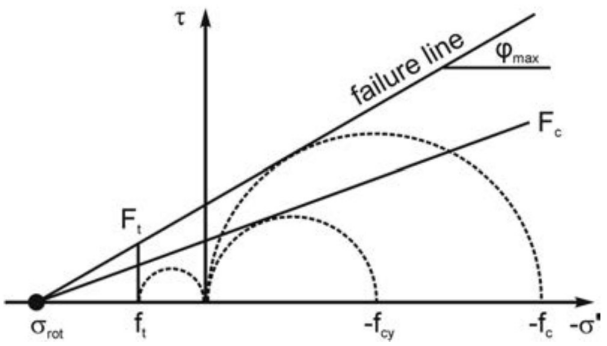

Figure 2.10: Yield surface and failure envelop of Shotcrete (Schädlich and Schweiger, 2014)

The combined Mohr-Coulomb and Rankine failure envelope was compared with experimental data on concrete (Kupfer and Gerstle, 1973). In the report, there was a good overall match with lab results. However, was is found that the material compression strength is underestimated by approximately 20% in bi-axial stress state.

The stress-strain curve was proposed by Schütz et al., 2011. They argued that since Shotcrete utilizes time-dependent behavior, the stress-strain curves should be normalized to account for that the strength varies with time. The normalized strain parameter for compression is $H_c = \varepsilon_3^p / \varepsilon_{cp}^p$. ε_{cp}^p is the plastic peak strain in uniaxial compression and ε_3^p is the minor plastic strain. The plastic peak strength ε_{cp}^p is derived from F_c and is a material property. Furthermore, the normalized stress parameter is the principal stress σ_3 divided by the uniaxial compressive peak strength f_c.

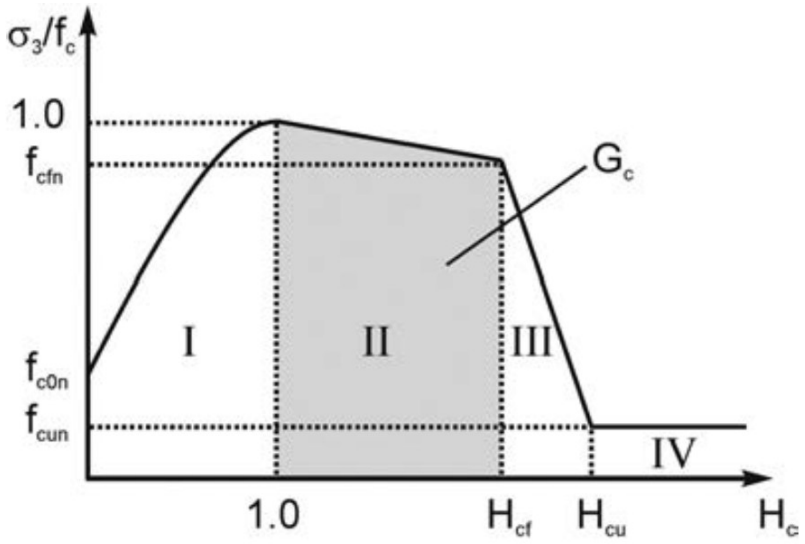

Figure 2.11: Normalized stress strain curve in compression (Schädlich and Schweiger, 2014)

The stress-strain curve is divided into four different parts (see Figure 2.11). In part I, the uniaxial yield strength f_{cy} is determined by the quadratic strain hardening function.

$$f_{cy,I} = f_c * (f_{c0n} + (1 - f_{c0n}) * (2H_c * H_c^2) \tag{2.13}$$

f_{c0n} is the ratio of the initial yield strength and peak strength, f_{cy}/f_c. Note that the purely elastic strain is not visualized, since the graph begins at yield. Furthermore, f_{c0n} is the starting point of the curve. Part I ends and Part II is initiated when f_c is fully mobilized, and the stress parameter reaches unity which coincides with $H_c = 1$. Linear softening occurs and the strength reduction is assumed to be caused by destruction of inter-particle bonds. Therefore, a parallel shift of the Mohr-Coulomb failure envelope occurs (PLAXIS, 2019).

$$f_{cy,II} = f_c * \left(1 + (f_{cfn} - 1) * \frac{H_c - 1}{H_{cf} - 1}\right) \tag{2.14}$$

where $H_{cf} = \varepsilon_{cf}/\varepsilon_{cp}$. Furthermore, ε_{cf} is derived from fracture energy in compression G_c and the characteristic length of the finite element L_{eq}.

$$\varepsilon^p_{cf} = \varepsilon^p_{cp} - \frac{2G_c}{(1 + f_{cfn})f_c * L_{eq}} \tag{2.15}$$

Linear softening also occur in Part III similar to Part II. However, it is dependent on the elastic unloading and plastic strain energy. The normalized stress strain curve in part III is calculated with the following equation.

$$\varepsilon^p_{cu} = \varepsilon^p_{cf} - \frac{2 * f_c(f_{cfn} - f_{cun})}{E} \tag{2.16}$$

$$f_{cy,III} = f_c * \left(f_{cfn} + (f_{cun} + f_{cfn}) * \frac{H_c - H_{cf}}{H_{cu} - H_{cf}}\right) \tag{2.17}$$

Where $H_{cu} = \varepsilon^p_{cu}/\varepsilon^p_{cp}$. In part IV a constant stress strain rate is adopted for numerical purposes. However, in reality the material have lost all of its strength in this phase.

Since the ductile behavior of concrete increases with increasing confining pressure, the total peak strain $\varepsilon_{cp} = \varepsilon^p_{cp} + \varepsilon^e_{cp}$ is determined by input parameter a and confining pressure in compression triaxial test σ_1.

$$\varepsilon_{cp} = \varepsilon_{cp,UC}\left(1 + a * \frac{\sigma_1}{-f_c}\right) \tag{2.18}$$

In tension, the model adopts a Rankine yield surface. The behavior is linear elastic until the peak tensile strength f_t is reached. Thereafter linear softening is adopted. Similar to compression, the tensile softening parameter is normalized, $H_t = \varepsilon^p_1/\varepsilon^p_{tu}$, where ε^p_{tu} is the plastic ultimate strain in uniaxial tension and ε^p_1 is the major principal plastic strain. Also, linear softening is dependent on the fracture energy in tension.

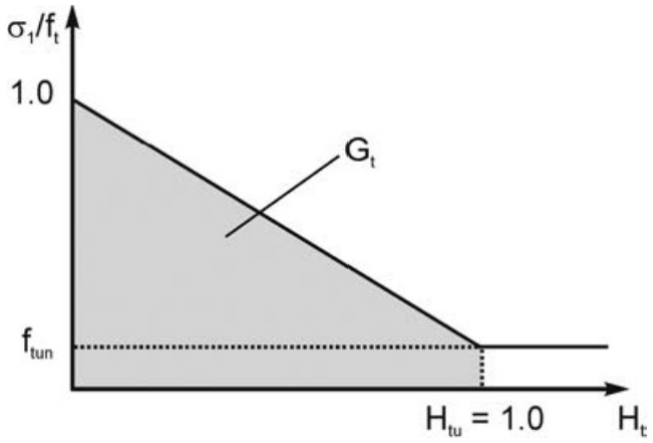

Figure 2.12: Normalized stress-strain curve in tension(Schädlich and Schweiger, 2014)

$$f_{ty} = f_t * (1 + (f_{tun} - 1)H_t) \tag{2.19}$$

$$\varepsilon^p_{tu} = \frac{2 * G_t}{(1 + f_{tun}) * f_t * L_{eq}} \tag{2.20}$$

2.3.3 Models for Soft Clay

Even though the focus of this thesis is the jet grouting material, there is still a need to model the soft soil accurately. This is because comparison will be usually made to actual deformation observed on site, thus it is important to model the entire system accurately. This section will explain why the MC model is insufficient to model soft clay behaviour. Instead, two different material models will be introduced to improve the model accuracy.

While the MC model explained in the previous section can also be used to model the soil, it is unable to accurately predict the behaviour of the soil behaviour. Firstly, the model assumes a linear elastic behaviour for the material. However, this does not reflect actual soil behaviour, where the stiffness degrades as the soil is loaded. This leads to an overestimation of the strength of the soil. Additionally, since the model only allows one input of Young's modulus, the model assumes that the unloading-reloading Young's modulus E_{ur} is the same as the initial Young's modulus (see Table 2.13). However, this is not true for actual soil behaviour in which the stiffness is stress-dependent, where the value of E_{ur} is much higher in the overconsolidated region the stiffness than in the normally consolidated region. This causes the model to over-predict soil heave for excavation problems.

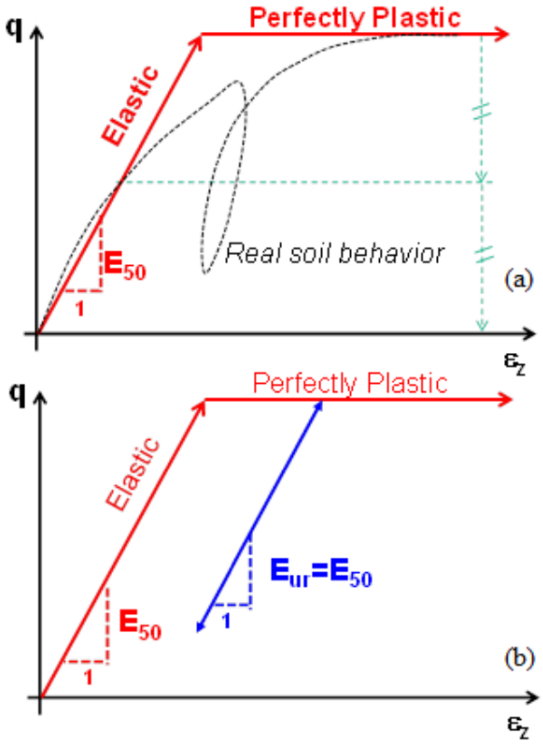

Figure 2.13: Assumption in the MC model (Gouw, 2014)

Furthermore, clays exhibit different hardening behaviour post-yielding depending on whether it is NC or OC. Thus, some kind of hardening rule will be required to be incorporated into the model to accurately predict the behaviour. These characteristics makes the Mohr-Coulomb model incompatible, as not only the model is unable to take into account the stress-dependency in the parameters, it also assumes a perfectly plastic behaviour.

2.3.3.1 Soft Soil Model

The Soft Soil (SS) model found in PLAXIS is based on the Modified Cam Clay (MCC) model (Roscoe and Burland, 1968). The MCC model using the p' and q stress invariants in the triaxial stress space where:

$$p' = \frac{1}{3}(\sigma'_1 + 2\sigma'_3) \quad , \quad q = \sigma'_1 - \sigma'_3 \tag{2.21}$$

$$\varepsilon_p = \varepsilon_1 + 2\varepsilon_3 \quad , \quad \varepsilon_q = \frac{2}{3}(\varepsilon_1 - \varepsilon_3) \tag{2.22}$$

In the MCC model, ε_p and ε_q are taken to be volumetric and deviatoric strains accordingly. In the elastic region, the volumetric and deviatoric strains are decoupled are given in the following matrix:

$$\begin{bmatrix} \delta\varepsilon_p^e \\ \delta\varepsilon_q^e \end{bmatrix} = \begin{bmatrix} \frac{1}{K'} & 0 \\ 0 & \frac{1}{3G'} \end{bmatrix} \begin{bmatrix} \delta p' \\ \delta q' \end{bmatrix} \tag{2.23}$$

In equation (2.23) K' is the volumetric modulus and G' is the shear modulus. However, K' is a function of the p' where $K' = K'(p')$. Generally, soils exhibit stiffness degradation with increasing pressure. Additionally, since the material is assumed to be isotropic in the yield surface, K' can be related to G', which means that G' is also a function of p' where $G' = G'(p')$. This makes the elastic behaviour to be non-linear unlike that assumed in the Mohr-Coulomb model.

In the MCC model, the yield surface is coupled with the failure surface and is given by using the following equation:

$$f(p', q, p'_0) = q^2 - M^2 p'(p'_0 - p') = 0 \tag{2.24}$$

In the equation (2.24), M relates to the stress ratio at critical state and thus represents failure. Additionally, the MCC model assumes an associative flow rule, which means that $g = f$.

The hardening rule for the MCC model is given as follows:

$$\frac{\delta p'_0}{\delta \varepsilon_p^p} = \frac{\nu p'_0}{\lambda - \kappa} \quad , \quad \frac{\delta p'_0}{\delta \varepsilon_q^p} = 0 \tag{2.25}$$

While the MCC model is able to accurately predict the behaviour of soils at critical state, the model fails to predict the behaviour in normal condition, especially for NC clay. This is because of the associated flow rule assumed in the MCC model, which results in high, unrealistic K_0 values.

The SS model differs from the MCC model by decoupling the plastic volumetric strain from the failure. Thus, the yield surface for the model is written instead using the following equation:

$$f_c = \frac{q^2}{(M^*)^2} + p'(p' - p'_0) = 0 \tag{2.26}$$

M^* in equation (2.26) is not the same as the M used in (2.24). Instead, M^* is calculated using the the K_0 values in the normally consolidated region, K_{0NC}. The value of K_{0NC} is often calculated using Jaky's formula using the critical state angle ϕ'_{cr} i.e. $K_{0NC} = 1 - sin\phi'_{cr}$.

There is a need to define the failure surface in the SS model since the failure surface is decoupled from the yielding surface. In this case, the Mohr-Coulomb failure criterion for soft soil with almost no cohesion is used and is defined as:

$$f_f = \frac{1}{2}(\sigma'_3 - \sigma'_1) + \frac{1}{2}(\sigma'_3 + \sigma'_1)sin\phi' - c' cos\phi' \tag{2.27}$$

To ensure zero plastic volumetric strain at failure, non-associative flow rule is thus assumed in the SS model with the value of the dilatancy angle ψ' set to 0^o for soft soils. Additionally, tension cutoff is introduced to remove the possibility of having tractions, which is unrealistic for soils.

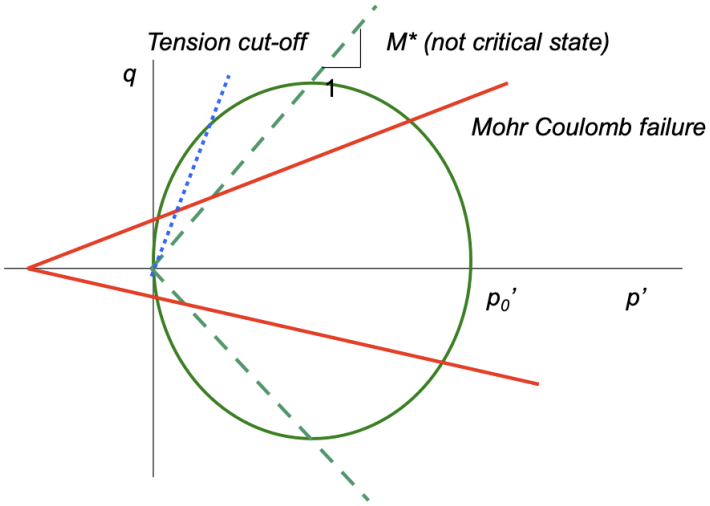

Figure 2.14: Yield Surface in the SS model (Karstunen and Amavasai, 2017)

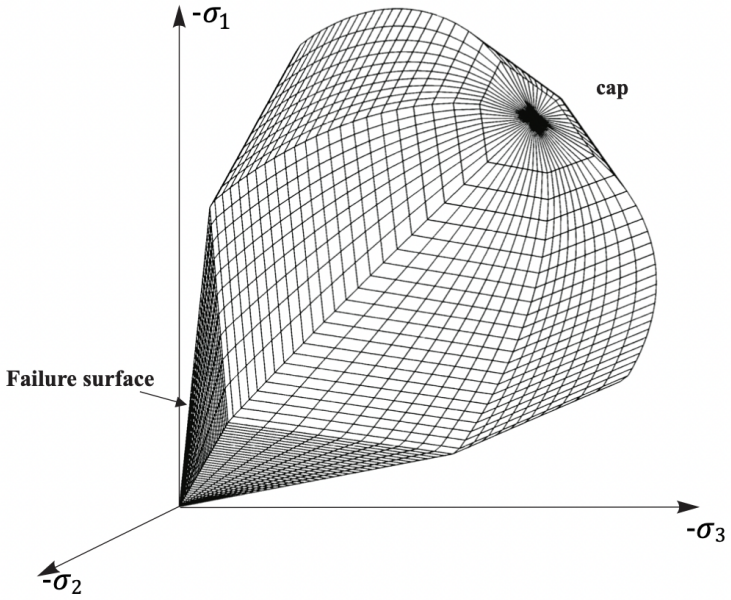

Figure 2.15: Failure Surface in the SS model in the principal stress space (PLAXIS, 2019)

The initial size of the yield surface for the SS model is dependent on the pre-consolidation pressure p'_0. In PLAXIS, this is controlled by inputting a value for the parameter overconsolidation ratio (OCR) or the pre-overburden pressure (POP) defined as $\frac{\sigma'_c}{\sigma'v}$ and $\sigma'_c - \sigma'_v$ respectively where σ'_c is the pre-consolidation pressure and σ'_v is the in-situ vertical effective stress. It is important to note that the output of the model using Soft Soil model is highly sensitive to the input of the OCR/POP (Karstunen and Amavasai, 2017). When yielding occurs, the yield surface will increase as a function of the plastic volumetric strain until the Mohr-Coulomb failure

criterion is reached.

To fully describe the relationship in the SS model, two parameters are introduced which are the modified compression index λ^* and modified swelling index κ^* which are obtainable from a semi-log scale of volumetric strain against the natural log of the vertical effective stress. This is different to the parameters λ and κ used in the MCC model as they are based on the void ratio. Lastly, a Poisson's ratio for the unloading/reloading ν_{ur} is introduced to fully explain the elastic relationship. Using all these parameters helps to separate the primary loading and unloading/reloading, a feature that is missing in the Mohr-Coulomb model.

2.3.3.2 Hardening Soil Model

The Hardening Soil (HS) model (Schanz et al., 2000) is a complex constitutive model that is originally aimed to improve the then-popular hypo-elastic Duncan-Chang model (Duncan and Chang, 1970) by modelling the non-linear stress-strain behaviour using an elasto-plastic model, thus having the ability to separate the loading and unloading stage. The model uses a multi-function yield surfaces which takes into account both shear and cap hardening. Shear hardening models the plastic strain due to primary deviatoric loading, whereas the cap hardening models that due to primary compression in isotropic or oedometer loading.

As explained in the previous section, soils tend to exhibit stiffness degradation (see Figure 2.13). This results in a hyperbola stress-strain relationship. The model is controlled by two different stiffness parameters, $E_{50}^{'ref}$ and $E_{ur}^{'ref}$. $E_{50}^{'ref}$ controls the stiffness in the primary loading, whereas $E_{ur}^{'ref}$ controls the stiffness in the unloading/reloading. Both stiffness parameters are stress-dependent which is behaviour that closely reflect that of soil. The power of this stress-dependency can also be controlled using the parameter m. For soft soil, a value of 1.0 should be picked to reflect the hyperbolic stress-strain relationship.

The yield functions for the shear hardening are given using the following equations:

$$f_i = \frac{q_a}{E_{50}^{'}} \frac{(\sigma_1^{'} - \sigma_i^{'})}{q_a - (\sigma_1^{'} - \sigma_i^{'})} - \frac{2(\sigma_1^{'} - \sigma_i^{'})}{E_{ur}^{'}} - \varepsilon_q^p \tag{2.28}$$

$$\varepsilon_q^p = \varepsilon_1^p - \varepsilon_2^p - \varepsilon_3^p = 2\varepsilon_1^p - \varepsilon_p^p \approx 2\varepsilon_1^p \quad , \quad q_a = \frac{q_f}{R_f} \tag{2.29}$$

q_f refers to the ultimate deviatoric stress, while R_f is a stress ratio defining the relationship between q_f and q_a and is defaulted to the value of 0.9.

Non-associated flow rule is assumed for the shear hardening yield function. Therefore, the plastic potential functions need to be defined using the following equations:

$$g_i = \frac{(\sigma_1^{'} - \sigma_i^{'})}{2} - \frac{(\sigma_1^{'} + \sigma_i^{'})}{2} sin\psi_m^{'} \tag{2.30}$$

$\psi_m^{'}$ is the mobilised dilatancy angle and it can be derived from the failure friction angle $\phi_p^{'}$ and critical friction angle $\phi_{cr}^{'}$. The following equations explain these process:

$$sin\psi_m^{'} = \frac{sin\phi_m^{'} - sin\phi_{cr}^{'}}{1 - sin\phi_m^{'} sin\phi_{cr}^{'}} \tag{2.31}$$

$$sin\phi_m^{'} = \frac{\sigma_1^{'} - \sigma_3^{'}}{\sigma_1^{'} + \sigma_3^{'} - 2c\cot\phi_p^{'}} \tag{2.32}$$

The shear hardening is capped by the Mohr-Coulomb failure criterion.

A cap yield surface is then added to complete the model. This cap aims to explain the plastic volumetric strain observed in isotropic compression. Another stress-dependent stiffness parameter $E_{oed}^{'ref}$ is introduced to control the magnitude of plastic strain from isotropic compression. This cap yield surface has the following function:

$$f_c = \frac{\bar{q}^2}{M^{*2}} + p^{'2} p_c^{'2} \tag{2.33}$$

$$\bar{q} = \sigma_1^{'} - \sigma_2^{'} - \sigma_3^{'} \tag{2.34}$$

In equation (2.33), M^* has the same function as that found in the SS model. For the cap yield surface, associated flow rule is assumed, thus $g_c = f_c$.

The hardening rule of the cap yield surface is controlled by the pre-consolidation pressure $p_c^{'}$ using the following formula:

$$\varepsilon_p^c = \frac{H}{m+1}\left(\frac{p_c^{'}}{\sigma^{'ref}}\right)^{m+1} \quad ; \quad H = \frac{K_c}{K_s - K_c} K_s \tag{2.35}$$

K_c and K_s are the elasto-plastic compression modulus and elastic swelling modulus respectively.

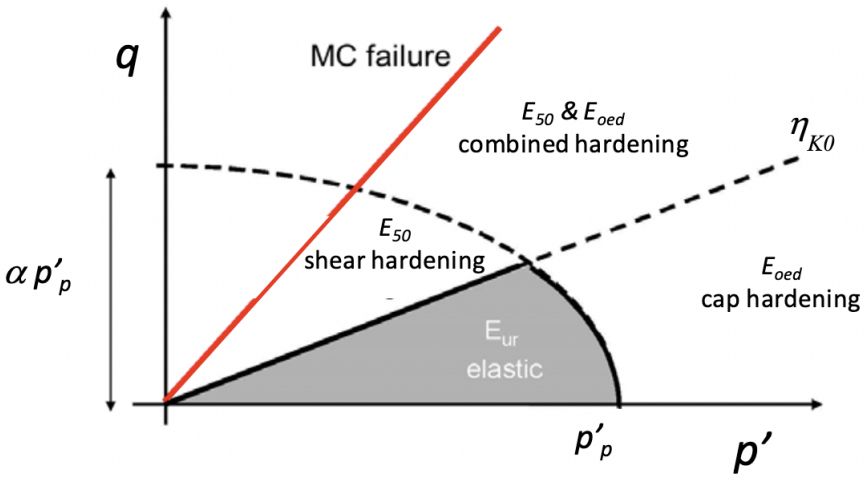

Figure 2.16: Yield Surface in the HS model (Karstunen and Amavasai, 2017)

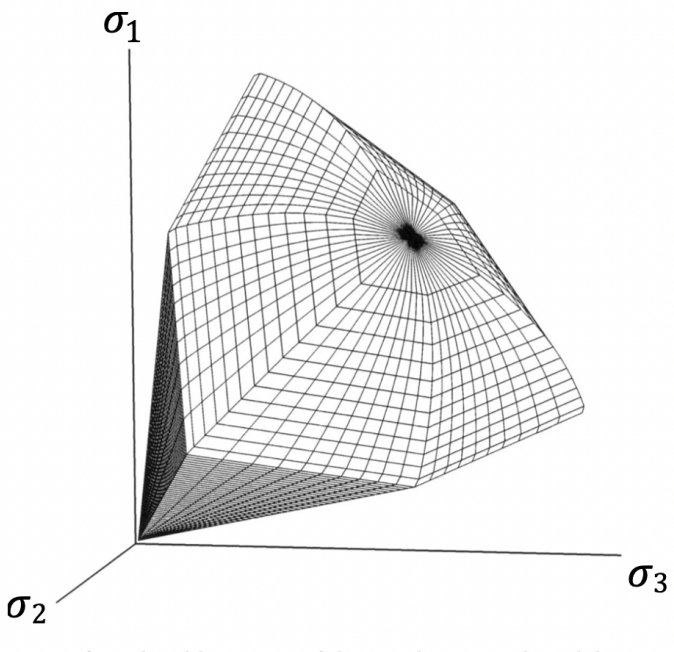

Figure 2.17: Failure Surface in the HS model in the principal stress space(PLAXIS, 2019)

3
Methodology & Setup

This chapter will first introduce the site that will form as a basis for analysis performed in this thesis. Conducted tests are then explained and how the model parameters are obtained. Last, but not least, the model setup in PLAXIS will be explained.

3.1 Study Site

The study site is located in Oslo, Norway for Oslo University Hospital which is one of the major hospital in Norway. Excavation up to 6m deep will be carried out for the project. To support the excavation, sheet pile wall retaining structures with anchors will be installed except for a small portion in the west side of the excavation, where jet grouting secant pile wall will be installed instead to minimise soil movement which can affect the adjacent buildings. Thirteen boreholes were conducted for the project and the information was used to understand the stratigraphy of the underlying soil. See Figure 3.1 for the cross-section of the excavation. As part of the construction, a part of the hospital was demolished (see Figure 3.2 below).

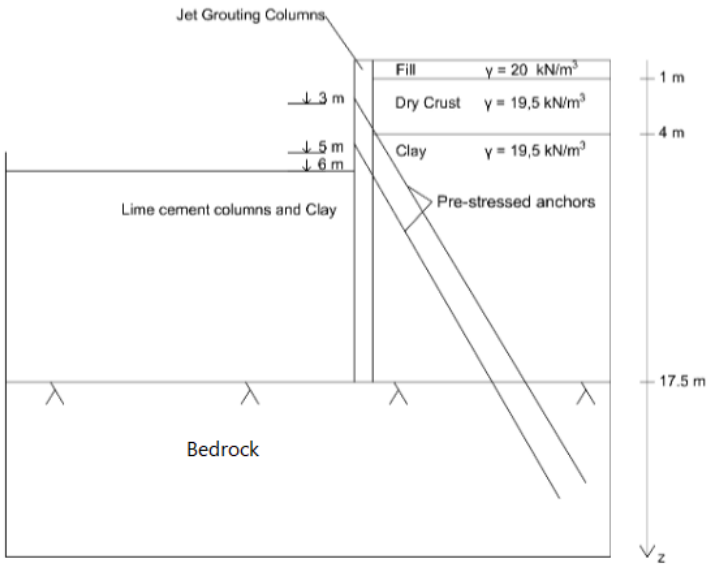

Figure 3.1: Cross-section of jet grouting construction

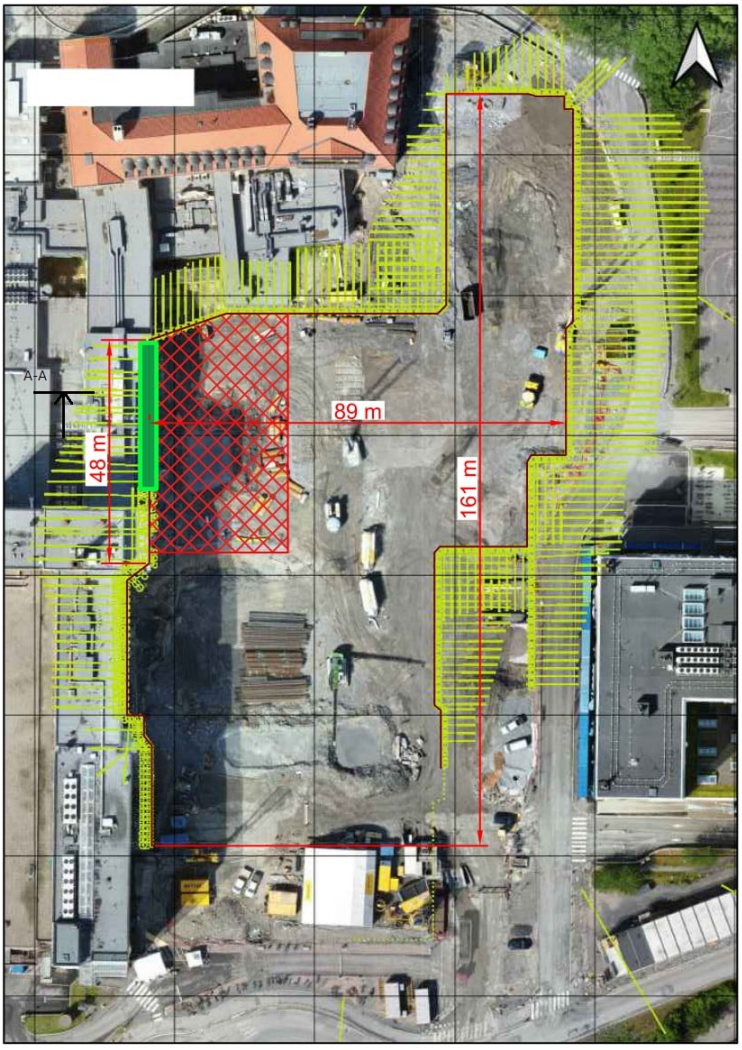

Figure 3.2: Overview of the excavation site. Secant jet grouting wall studied is within the green rectangle. The red hatched area represent the demolished section of the building and the yellow lines are the anchors (after Keller, 2021)

Information on the existing foundation of the hospital is limited. Therefore, they are some assumptions made in the geotechnical investigation report. The foundation of the demolished section is assumed to be direct foundation, whereas the surrounding structures around the excavation are assumed to be on pile foundations (Norconsult, 2019). The main geotechnical challenge with the expansion was the risk of damaging adjacent structures due to their close proximity. Therefore, a jet grouted secant pile wall was utilized along the west excavation wall to minimize settlements on the adjacent building and provide excavation support. To further secure the excavation against displacement and basal heave, lime-cement (kalkcement in Swedish, hereafter abbreviated as KC) columns were constructed on the base of the excavation (Norconsult, 2019).

Instrumentation is done to measure the deflection and displacement of the secant

wall which includes an inclinometer on the adjacent sheet pile walls. Unfortunately, field measurement data are not available for this thesis.

3.2 Geotechnical Site Analysis

3.2.1 Original Ground Investigation

A ground investigation was conducted by Øvre Romerike Prosjektering AS (ORP, 2017. Thirteen boreholes was conducted (see Figure 3.3). Undisturbed samples were retrieved in the clay layer from boreholes 3, 8 and 9 at a depth of 6-7m for laboratory testing. Table 3.1 tabulates the tests schedule conducted in the original geotechnical investigation.

Figure 3.3: An overview of the site with borehole location (after ORP, 2017)

Table 3.1: Tests Schedule in Original Ground Investigation

Test Name	Quantity	Test Type
Total sounding	13	In-situ test
CPTu	3	In-situ test
Physical properties test	29	Lab test on clay
Atterberg Limits	9	Lab test on clay
Organic content	9	Lab test on clay
UCS	25	Lab test on clay
Oedometer CRS	4	Lab test on clay
Triaxial CAUa	4	Lab test on clay
UCS	12	Lab test on KC
UCS	14	Lab test on jet grout

The field test consisted of total soundings and Cone Penetration Tests with piezometer data (CPTu). These field tests give approximation of the soil layering, strength, groundwater level and bedrock depth.

Laboratory testing was conducted by Multiconsult ASA in Oslo. Tests were conducted to determine the physical properties of the clay, which include its Atterberg limits and organic content. Twenty-five UCS tests and 4 consolidated anisotropic undrained active (CAUa) triaxial test were conducted to determine the mechanical properties of the clay, which will form as the main data for this thesis. The term "active" is used in Norwegian standard to denote compression loading.

Uniaxial compression tests (UCS) were done on the KC columns. Two different mixtures were tested, 80 kg/m^3 and 100 kg/m^3. In total 16 tests were conducted where the mixtures was cured for 7 days and 22 days.

UCS for the jet grouting material were conducted by Keller Grundläggning AB within the studied section. The test conducted was cured for 3, 13 and 37 days with a total of 14 tests done.

3.2.2 New Laboratory Test on Jet Grout Material

Additional jet grout samples were needed to find material properties that will be required as model parameters for the Shotcrete material model. However, due to logistical limitation, samples for jet grouting were retrieved for another construction site in Stockholm instead.

It is noted that the jet grouting primary function in the Stockholm site is to reduce permeability, and thus the strength is of less importance. Therefore, even though the jet grout is of the same specification as that of Oslo site, the strength quality is not highly controlled and thus may vary greatly.

Table 3.2 tabulates the additional tests schedule. Samples for UCS and wedge splitting test (WST) were taken and testing was conducted in Chalmers laboratory. The samples was collected through the spoil of the jet grouting rig. Four 150mm cube samples were retrieved for UCS, whereas 3 cube samples were collected for WST. UCS were conducted to compare the strength difference between the jet grout used in the Stockholm site and the study site, while WST were done to determine the fracture energy G_c and G_t which is required for the Shotcrete material model (Brühwiler and Wittmann, 1990). The samples are left to cured for 28 days to ensure that the strength of the concrete has fully developed. The properties at the 28^{th} days are also part of the model parameters for Shotcrete model.

Table 3.2: Additional Test Schedule from Stockholm Site

Test Name	**Quantity**	**Test Type**
UCS	4	Lab test on jet grout
WST	3	Lab test on jet grout

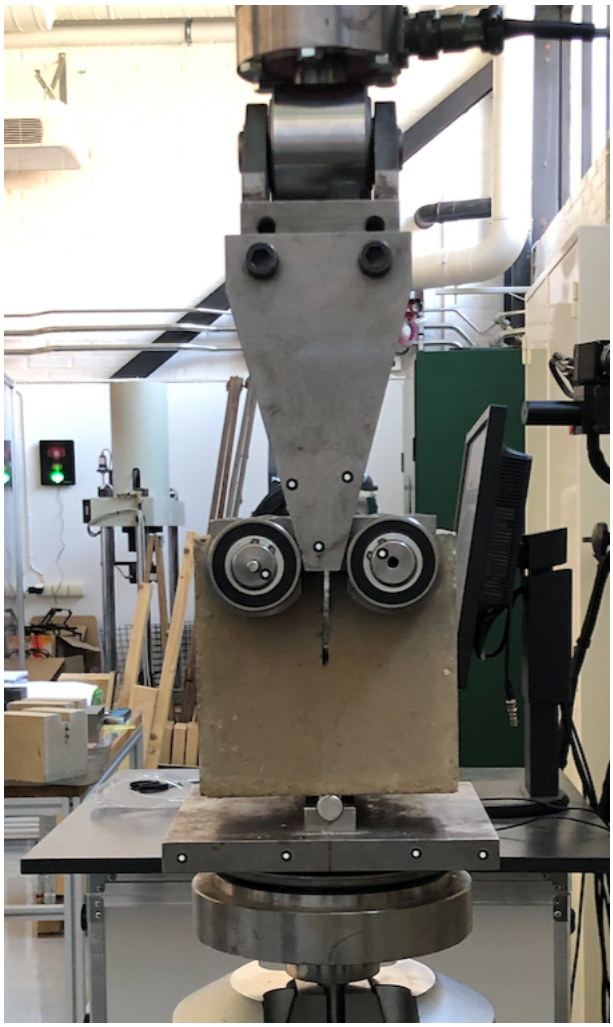

Figure 3.4: Picture of a wedge splitting test conducted in Chalmers

The process of sampling and testing for WST was done according to Brühwiler and Wittmann, 1990. The sample are cast with a groove to make space for loading devices with rollers. After the samples are cured, preparation can be initiated by sawing a notch along groove, in the center. The notch directs the fracture vertically. Then, the loading devices with rollers are placed on top of the samples (see Figure 3.4). On the upper plate of the loading machine, two wedges are fixed. The test can now be performed by applying force on the upper plate. During the test the applied load F_v and crack opening displacement (COD) are measured. The COD are measured with a clip gauge that was fixed in the in the same level where the splitting fore is acting i.e same level as the rollers. The applied load is controlled by the COD. The test in finished when no significant force can be record. The test present the result in a splitting force F_v-COD displacement graph.

3.3 Derivation of model parameters

In this section the method to derive the model parameters is presented. The procedure to obtain the input data when available is described in the previous section. SoilTest will be utilised to validate the model parameters against the actual laboratory data. Lastly, a KC-clay composite material will be created to better reflect the site condition.

3.3.1 Data from CRS Tests

Stress-strain relationship from the CRS test is used to obtain the modified compression index λ^* and modified swelling index κ^* for the SS model. A semi-log stress-strain graph was plotted where the axial stress is in natural logarithmic scale. κ^* and λ^* can then be found as they are the stress-strain ratio along the primary compression curve and the virgin compression curve accordingly (see Figure 3.5). Determination of κ^* and λ^* requires a graph of stress against volumetric strain, however it is assumed in this thesis that the samples are fully constrained in the horizontal axis. Therefore, any volumetric strain that occurs in the test can be fully attributed to the axial strain.

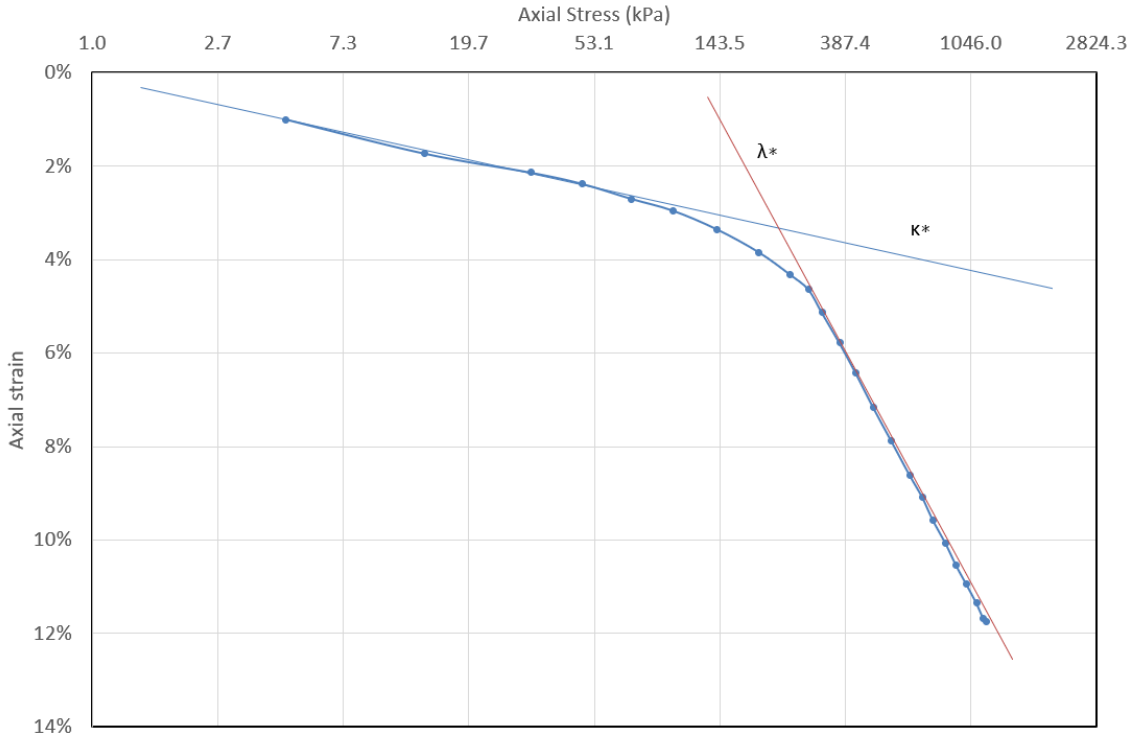

Figure 3.5: Method to find the modified compression index and modified swelling index λ^* and κ^*

As mentioned in the previous chapter, the preconsolidation pressure $p_0^{'}$ is an important parameter for the SS model. This can be determined from the CRS test using a simplified method. This is performed in a semi-log stress-strain graph where the axial stress is in base-10 logarithmic scale. The straight part in the elastic region is extended forward, whereas the straight part in the plastic region is extended backward. The stress value of the intersection of these two lines gives the value for σ_c (see Figure 3.6).

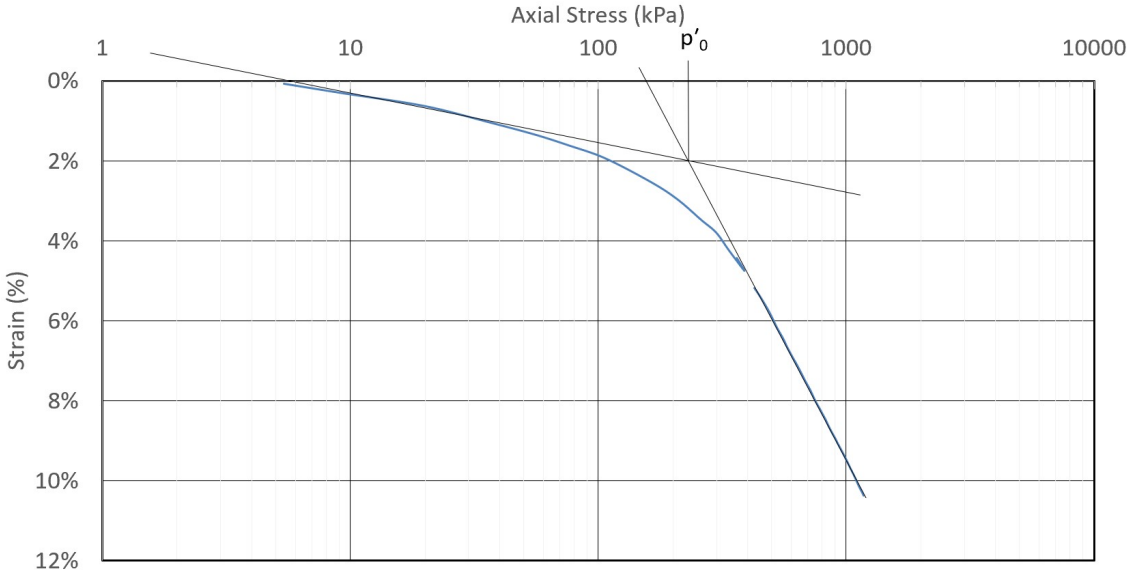

Figure 3.6: Simplified method to determine preconsolidation pressure p'_0

3.3.2 Data from Triaxial Tests

A p'-q plot was retrieved from the CAUa tests where $p' = (\sigma_r^{'} + 2\sigma_a^{'})/3$ and $q = (\sigma_a^{'} - \sigma_r^{'})$. In principal stress notation, $\sigma_a^{'} = \sigma_1^{'}$ and $\sigma_r^{'} = \sigma_2^{'} = \sigma_3^{'}$. The critical friction angle $\phi_{cr}^{'}$ can be obtained from the p'-q plot by first drawing a best-fit failure envelope matching the laboratory data drawn from the origin (see Figure 3.7). Since the tests are compression tests, the slope of the failure envelope gives the value of M_c. $\phi_{cr}^{'}$ can then be derived using the following formula:

$$sin\phi'_{cr} = \frac{3M_c}{6 + M_c} \tag{3.1}$$

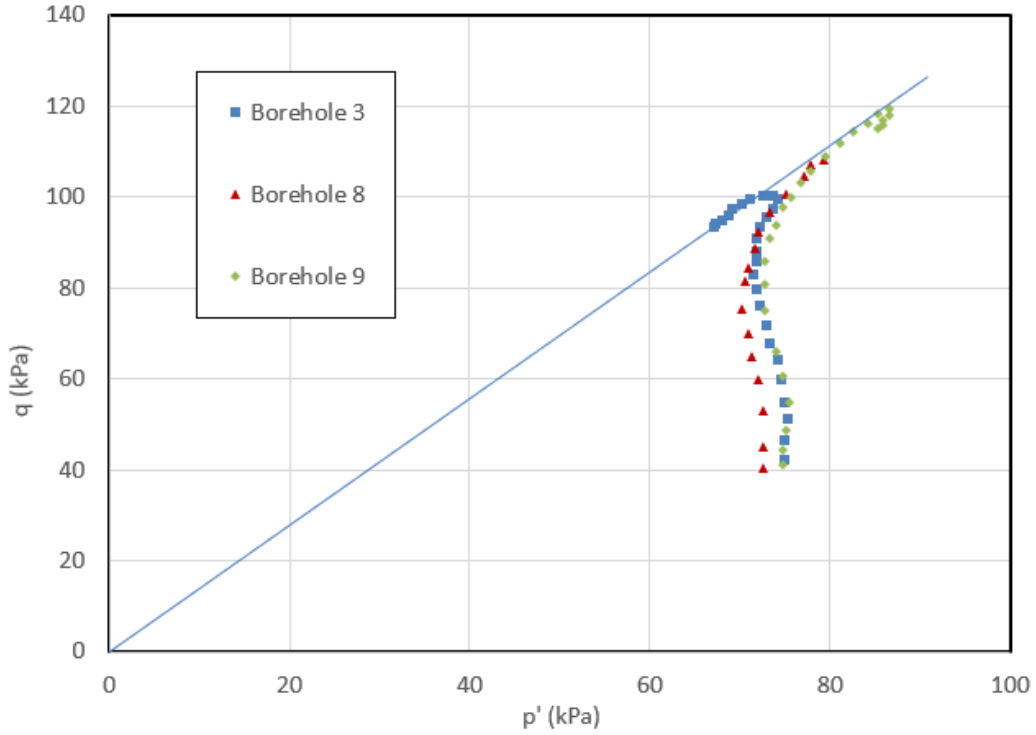

Figure 3.7: Method to find the slope of the critical line M_c.

UCS results for the jet grout conducted in Chalmers can be seen in Figure 3.8. During the sampling process, "UCS 1" was slightly damaged and fractures appeared on the cube (see Figure 3.9). This explains the lower peak strength observed for "UCS 1" in comparison to the other samples. The Shotcrete model parameter uniaxial compressive strength $f_{c,28}$ was calculated by identifying the peak stress divided by the sample area.

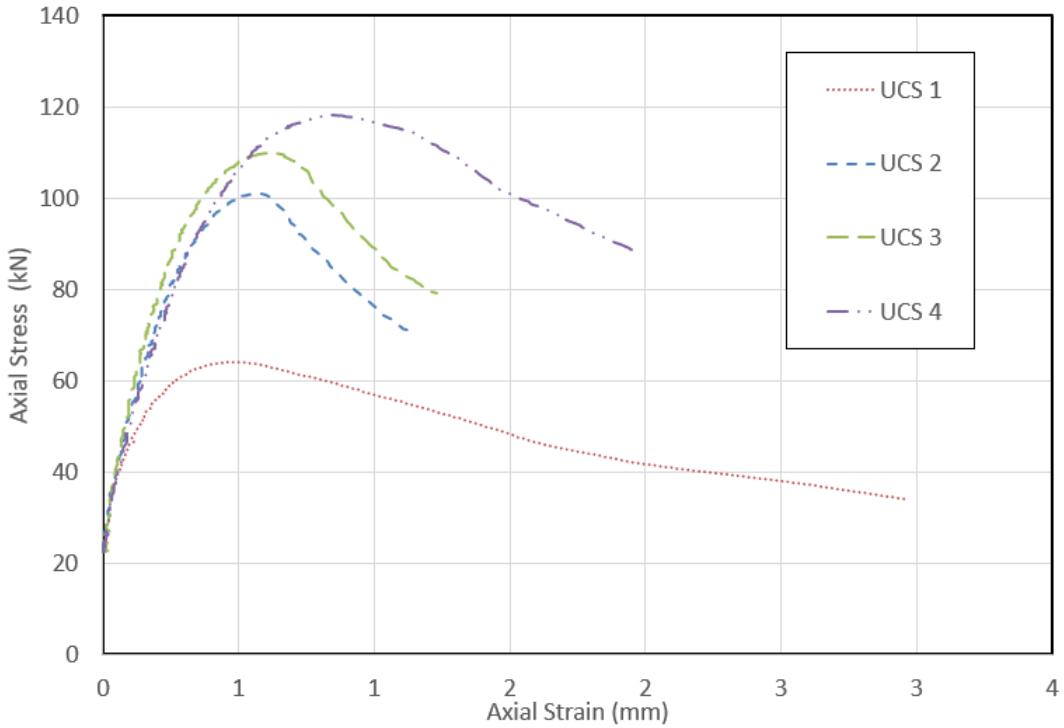

Figure 3.8: Uni-axial compression test in conducted in Chalmers for jet grout material

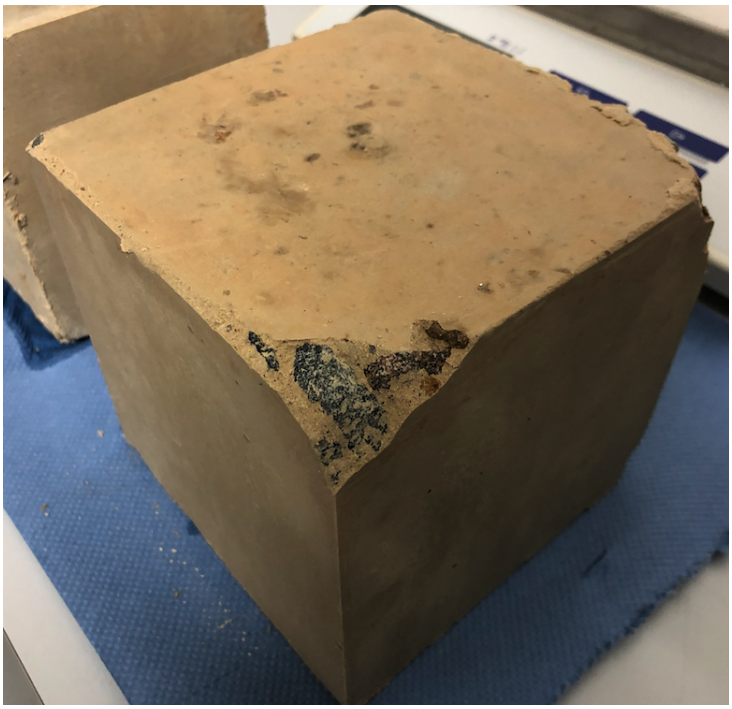

Figure 3.9: Sample quality of UCS1

3.3.3 Data from WST

The procedure of calculating the fracture energy was done according to Brühwiler and Wittmann, 1990. The test results are presented as splitting force F_v against COD measurement. The aim of the WST is to measure the necessary energy to split the samples. The energy is represented by calculating the area under the F_v-COD graph. The energy divided by the fracture area is the specific fracture energy G_f. According to Brühwiler and Wittmann, 1990, G_f has a similar value to G_t and to remain conservative, $G_c = G_t$ is assumed.

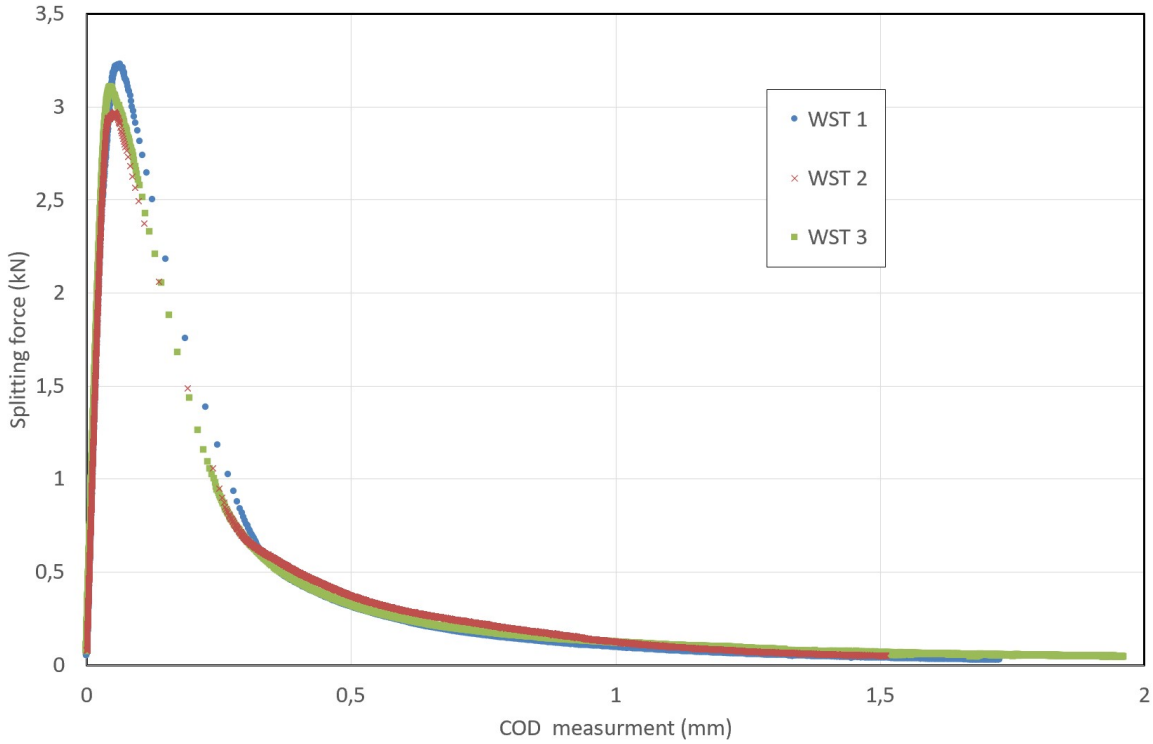

Figure 3.10: Results of the wedge splitting test

3.3.4 Model Parameters Completion

Many model parameters required for the Shotcrete model were not obtainable from the test data that were both provided for and conducted. Therefore, assumptions and literature reviews were conducted to determine these parameters.

The unit weight of the jet grouts γ is assumed to be the same as that of concrete which is equal to 25kN/m^2. Additionally, since no tensile tests were conducted, the uniaxial tensile strength is assumed to be related to the compressive strength using the following equation based on (IS456:2000, 2000):

$$f_{t,28} = 0,7\sqrt{f_{c,28}} \tag{3.2}$$

For the other missing model parameters for the Shotcrete model, the values recommended by the PLAXIS manual is adopted (PLAXIS, 2019).

Since laboratory tests were only conducted for the clay layer, values from literature reviews in the vicinity will be used to determine the model parameters required for the fill, dry crust, and the bedrock layer.

The bedrock model parameters were obtained from the Kværnerdammen F1 project where lab tests and a Plaxis model were conducted (MulticonsultASA, 2017). The project is located in Oslo and is approximately 6 km away from the study site.

Model parameters for fill and dry crust were retrieved from Rødvand et al., 2019 where the researchers studied a case of a road bridge hit by a landslide in sensitive clay. The accident occurred on the Mofjellbekken located approximately 50 km south of Oslo.

Table 3.3: Retrieved values from literature values

Layers		Fill material	Dry crust	Bedrock	Unit
General					
Material model	*Type*	MC	MC	Linear elastic	
Total unit weight	γ	20	19,5	19,5	kN/m^3
Parameters					
Young's modulus	E	30 000	30 000	1 300 000	kPa
Odometer stiffnes	E_{eod}^{ref}	-	-	1 750 000	kPa
Poisson's ratio	ν	0,4	0,4	-	
Friction angel	ϕ	38	38	-	°
Dilantancy angel	ψ	0	0	0	°

The design undrained shear strength s_u requirement for the lime cement columns is 100 kPa. This was validated by the UCS tests conducted in the original geotechnical investigation by Keller. However, Hardening Soil model parameters could not be obtained from UCS. Therefore, the Hardening Soil model parameters for lime cement columns were determined according to (Ignat et al., 2020) using the following equations, where the power of stress level dependency is $m = 0.7$:

$$E_{50}^{'ref} = 1120 s_u \tag{3.3}$$

$$E_{oed}^{'ref} = E_{50}^{'ref} \tag{3.4}$$

$$E_{ur}^{'ref} = 3E_{50}^{'ref} \tag{3.5}$$

3.3.5 Sample Quality

Prior to validation of the model parameters obtained from actual laboratory test data, the quality of the samples from which the actual test data are derived from needs to be assessed.

Ideally, laboratory tests need to be conducted on undisturbed samples. This is to ensure that the samples reflect a condition and stress state that is identical when they are found in the ground. This is especially true for clay as its behaviour is highly dependent on its stress history as explained in the previous chapter.

In reality, while efforts are taken to minimise disturbance to the samples, obtaining one that is perfectly identical to that found in the ground is very difficult. Thus, there is a need to qualify the quality of the undisturbed. The two commonly used grading criteria are Specimen Quality Designation (SQD) by Terzaghi et al., 1996 based on volumetric strain and $\delta e/e_0$ criteria by Lunne et al., 1997. These criteria help to rank the quality of the samples using the original condition as the baseline. For example, Terzaghi et al., 1996 mentioned that for oedometer tests, samples should have a quality of B at the minimum. While these criteria are primarily used for oedometer samples, they can still be used to determine the overall sample quality. The table below shows the quality of the samples collected based on these two criteria.

Table 3.4: Original Geotechnical Investigation Sample Quality

Samples Quality				
Borehole	**SQD**	**SQD Quality**	δ**e**/δ**e$_0$**	δ**e**/δ**e$_0$ Quality**
3	2,46%	C	0,056	Poor
8	2,14%	C	0,051	Poor
9	2,79%	C	0,069	Poor

As mentioned in the previous section, jet grout samples in the Stockholm site is collected from the spoil instead of jet grout core samples. The spoil is the backflow of jet grout as the columns are being cast. Thus, it is important to note that the sample collected will contain some impurities such as small rocks or soft clay that may make the samples less representative of those that are cast on site. This can be observed in Figure 3.11 which is taken post-WST. Additionally, air voids can be observed as well, which adversely affect the sample quality further. Nevertheless, it is not possible to obtain a clean cube sample with wedges from coring.

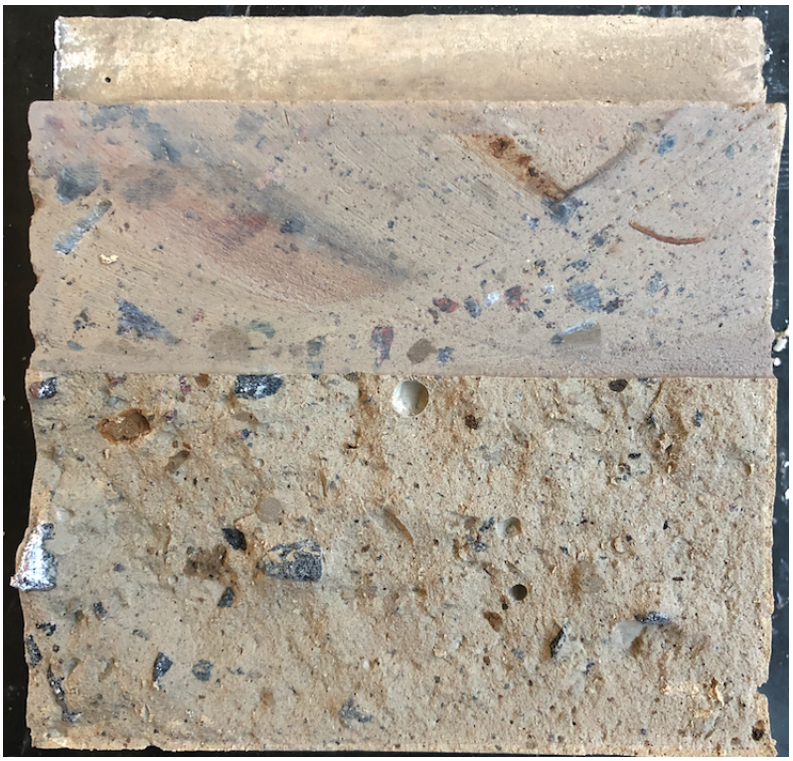

Figure 3.11: WST sample quality containing impurities and air voids

3.3.6 Model Parameters Validation

SoilTest is a tool found in PLAXIS that can simulate laboratory tests based on the model parameters. In this thesis, SoilTest was used to validate the model parameters derived for the the clay layer and KC columns against experimental results. Three different graphs were compared, one for oedometer CRS test simulation and two for triaxial tests simulation. Comparing the data (see Figure 3.12), the CRS simulation produces data that has an overall good match with the experimental data. However, a slight underestimation of the virgin compression line and the strain during preconsolidation is lower compared to experimental data.

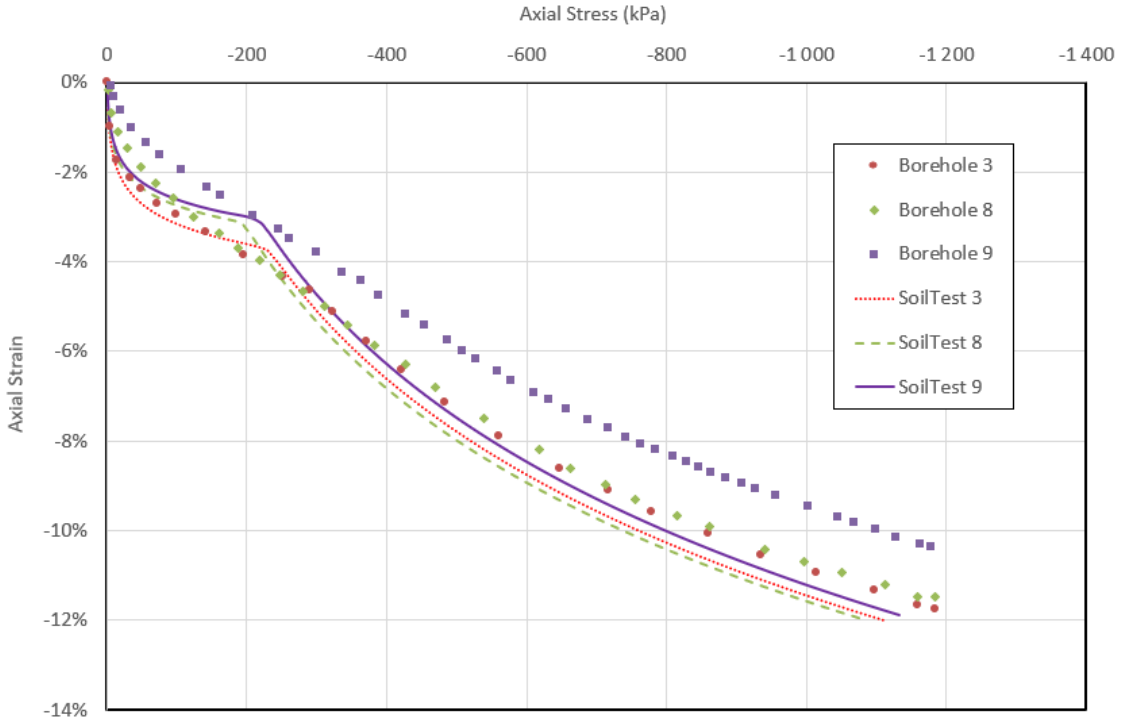

Figure 3.12: Strain-Stress graph CRS test and SoilTest.

For the triaxial tests simulation, the simulation produces data that are comparable to the actual data in the p'-q stress space (see Figure 3.13). However, in the q-strain plot, the simulation is underestimating the peak deviator stress for Boreholes 9 and 8, with 9 kPa and 16 kPa respectively and overestimate that for Borehole 3 with 4 kPa (see Figure 3.14. These differences are assumed to be attributed to the sample quality explained in the previous section.

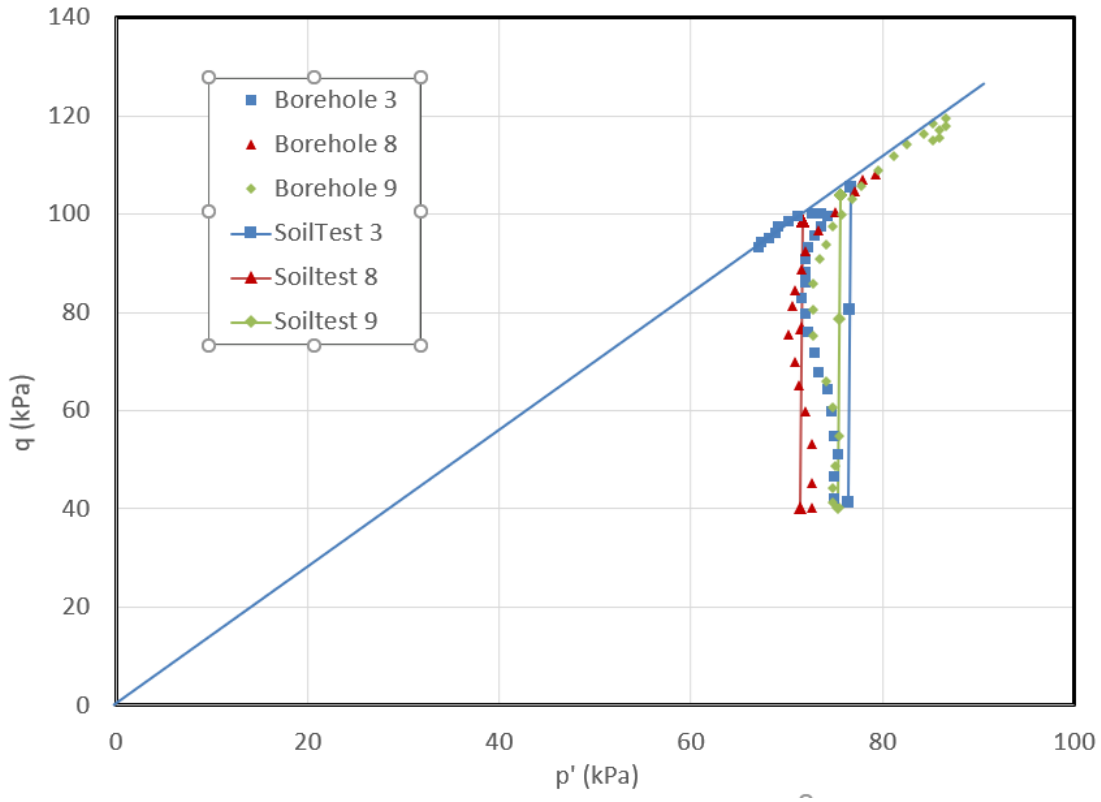

Figure 3.13: p'-q plot comparison between actual and simulation data

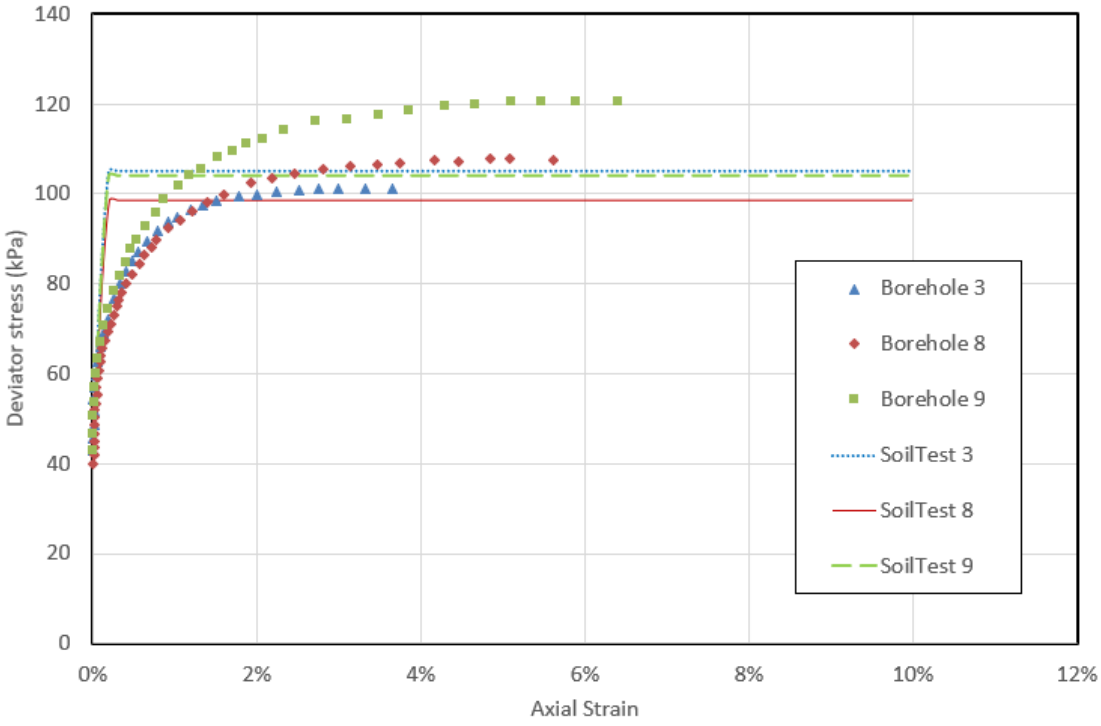

Figure 3.14: q-strain plot comparison between actual and simulation data

3.3.7 KC-clay Composite Material

KC columns were installed along west-east line in the study site (see Figure 3.15). The model that will be created in PLAXIS will be of a cross-section along the same line. However, Figure 3.15 shows that not the entire excavation is filled with KC columns. As such, using the model parameters of KC to model the material in PLAXIS will lead to an overestimation of the material strength.

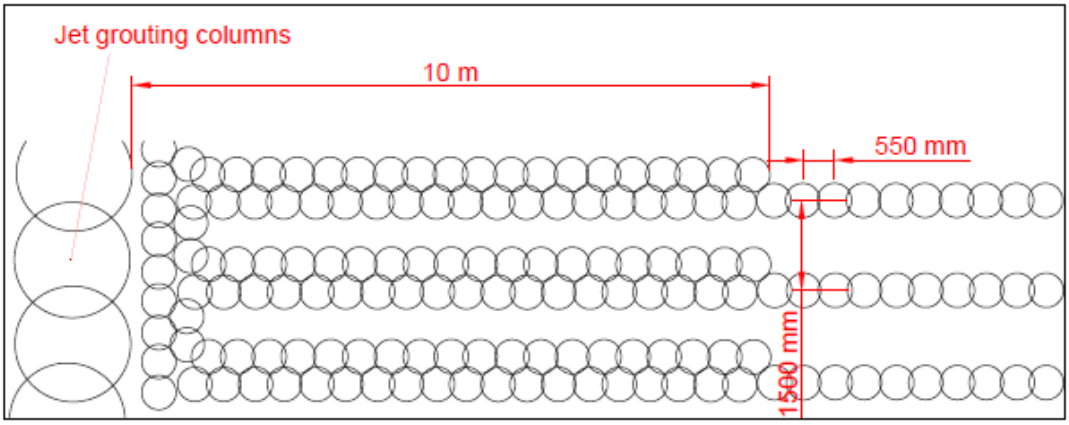

Figure 3.15: Drawing for placement of KC coloumn

This thesis proposed to introduce a KC-clay composite material to alleviate this problem. The material will be modelled using the HS model and the model parameters for the composite material were obtained using the ratio of clay and KC content according to Equation 3.6.

$$Composite\ parameter = Clay\ parameter * clay\ \% + KC\ parameter * KC\ \% \quad (3.6)$$

Two different composite materials were found with two different ratios of clay and KC. The composite nearer to the wall has a KC centre-to-centre spacing (c/c) that corresponds to 680 mm and a ratio of KC of 0.7. It stretches 10 m out from the from the excavation wall. The second composite material has a c/c of 1500 mm and KC ratio of 0,366.

Since the clay is originally modelled using the Soft Soil model, there is a need to find the equivalent model parameters for the clay for Hardening Soil model.

E_{50} for clay was first obtained using data from the triaxial CAUa tests. Note that all three CAUa has an initial deviatoric stress of approximately 40 kPa. The secant modulus E_{50} was obtained between the point where the test was initiated and 50 % of the peak strength q_f subtracted by the initial deviatoric stress.

E_{50} was then converted to E'_{50}. The ratio of E_{50}/E'_{50} is approximated to be between 3 to 4 (Lambe and Whitman, 1969). The difference is attributed to the fact that

there is no volume change in undrained loading, leading to lower axial strain. In this thesis, the ratio is to be taken to be equal to 3.

$E_{50}^{'ref}$ was then calculated with Equation 3.7. For soft soils, modulus component m of 1 and c of 0 is assumed. The value of $p_{ref}^{'}$ is 100 kPa which is the default value used in PLAXIS and $\sigma_3^{'}$ was obtained from the corresponding initial cell pressure of the test. Changing the value of $p_{ref}^{'}$ bears no significance to the outcome to the final result.

$$E_{50}' = E_{50}^{'ref}(\frac{\sigma_3' + a}{p_{ref} + a})^m \quad ; \quad a = c^{'} cot\phi^{'} \tag{3.7}$$

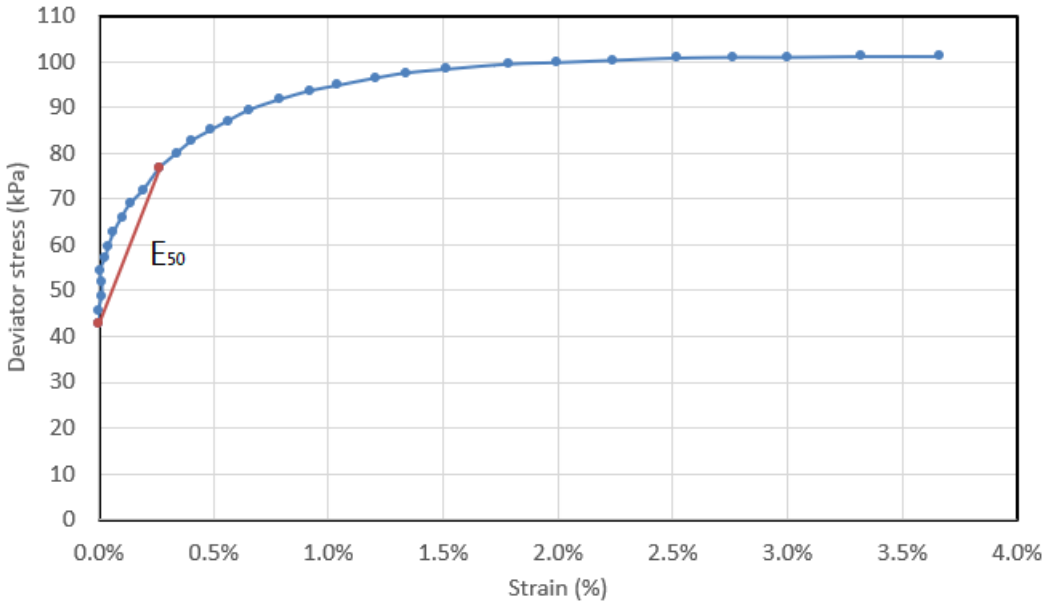

Figure 3.16: Method to find the E_{50}

Since the sample quality falls below the recommended SQD quality (Terzaghi et al., 1996) as seen in the previous section, E_{oed}' was obtained by using the equation found in the PLAXIS manual where $E_{oed}^{'ref} = \frac{p^{ref}}{\lambda^*}$ (PLAXIS, 2019).

Since the original triaxial CAUa tests lack the unloading/reloading loop, SoilTest tool was utilised to determine $E_{ur}^{'ref}$ where its value was found by matching the simulation data with the given data. The final match can be seen in Figure 3.17.

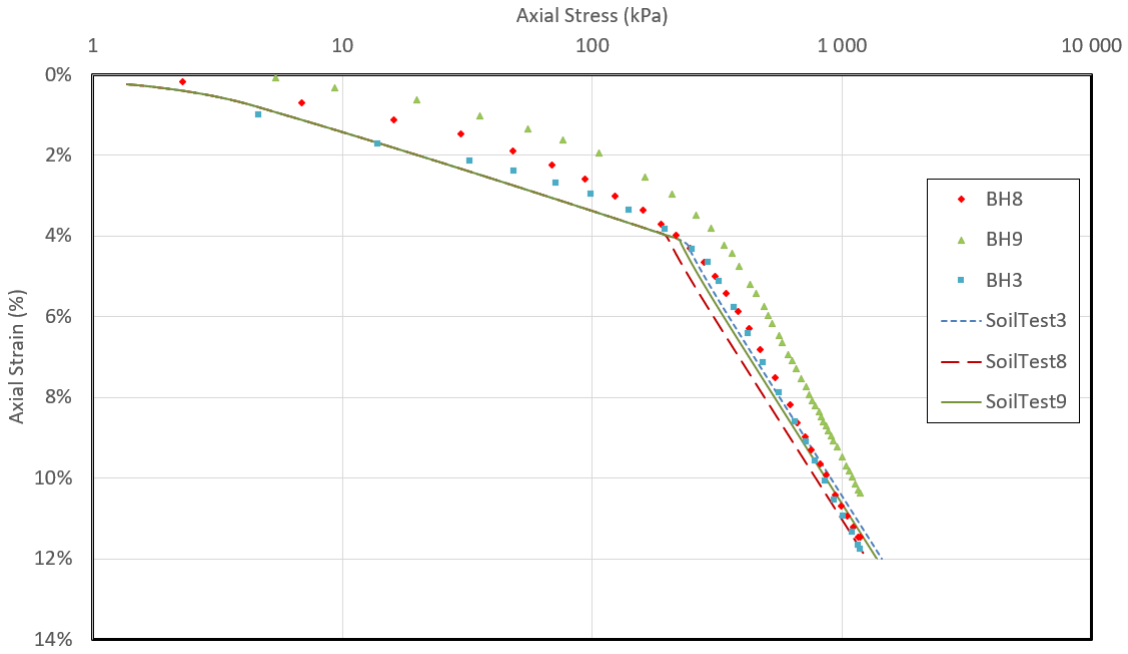

Figure 3.17: CRS Simulation of Clay using HS model

Using this method, it was found that $E_{ur}^{\prime ref}$ is approximately 5 times of $E_{50}^{\prime ref}$. This is different than the relationship found in the PLAXIS manual, where $E_{ur}^{\prime ref}$ is found to be 3 times of $E_{50}^{\prime ref}$ (PLAXIS, 2019). One possible reason to explain this observation is that the relationship found in the PLAXIS manual is calibrated to be more suitable with Dutch soils. Thus it may not fully represent the soils that are found in Norway.

3.4 Plaxis Model Setup

3.4.1 Model Geometry

PLAXIS 2D 2019 was used for the FEM in this thesis. The model is performed with 15-nodded triangular elements in plane strain analysis. The cross-section and soil-layering within the excavation site were obtained using boreholes done in the original ground investigation. On the other hand, the stratification outside the excavation is not known and is thus assumed to be the same as that found at the jet grout secant wall. Additionally, since adjacent buildings are founded using pile foundations up to the bedrock depth, they were not modelled in as they are assumed to have no effect on the soil's behaviour.

Symmetrical analysis is assumed, thus only half of the excavation is modelled which is 63,5m wide. This assumption may not hold especially since the bedrock depth is not known beyond the halfway point. Nevertheless, since the focus is on the deformation analysis of the jet grouting, base deformation on the other half of the excavation is of less importance for this thesis. The length of the active side of the excavation is assumed to be two times the excavation depth which is 6m deep. In total, the model is 75,5m wide cross-section. The deepest bedrock depth found in

this cross-section is 20m deep. Since the anchors are embedded 5m into the bedrock layer, the total depth of the model is 26m. Lastly, the groundwater level is located just above the dry crust at 3,5 m below the ground level. Figure 3.18 shows the model in PLAXIS.

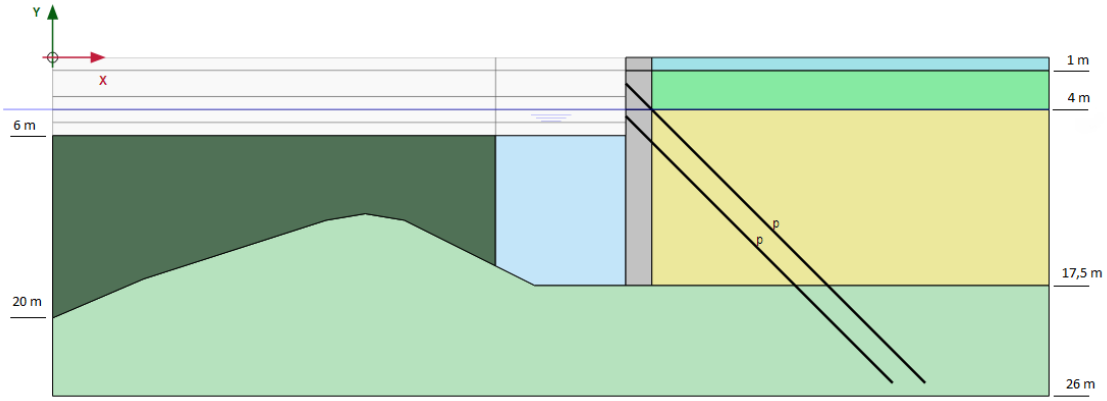

Figure 3.18: Cross-section of the model

The boundary conditions are defined where: 1) deformations are normally fixed on both sides, fully fixed on the bottom and free at the top; and 2) groundwater flow are open on the sides, closed for the bottom and opened at the top. Further, isothermal condition is assumed i.e. effects of temperature are not considered.

3.4.2 Input Parameters

Input parameters are tabulated in Table 3.5, 3.6 and 3.7 for soft soil, jet grouting and anchors respectively. Derivations of these parameters have been thoroughly discussed in the previous section and detailed calculations can be found in the Appendix (section A.1 to A.4).

Table 3.5: Model parameters for soil layers

Layers		Fill	Dry crust	Clay	KC c/c 680	KC c/c 1500	Bedrock	Unit
General								
Material model	*Model*	MC	MC	SS	HS	HS	Linear Elastic	
Drainage type	*Type*	Drained	Drained	Und.(A)	Und.(B)	Und.(B)	Non-porous	-
Unsaturated unit weight	γ_{unsat}	20	19,5	19,5	19,5	19,5	19,5**	kN/m^3
Saturated unit weight	γ_{sat}	20	19,5	19,5	19,5	19,5	19,5	-
Parameters								
Elastic stiffness	E' / E_{50}^{ref}	30 000*	30 000*	-	80 645	46 155	1 300 000**	kN/m^2
Odeometric stiffness	E_{eod}^{ref}	-	-	-	79 120	42 952	-	kN/m^2
Un-/reload stiffness	E_{ur}^{ref}	-	-	-	247 800	147 480	-	kN/m^2
Poisson's ratio	ν	0,3*	0,4*	-	-	-	0,25**	-
Undrained shear strength	$s_{u,ref}$	-	-	-	100	100	-	kN/m^2
Power of stress-level dependency	m	-	-	-	1	1	-	-
Modified compression index	λ^*	-	-	0,05276	-	-	-	-
Modified swelling index	κ^*	-	-	0,005337	-	-	-	-
Effective cohesion	c'_{ref}	1	1	-	-		- -	kN/m^2
Effective friction angle	ϕ	35*	38*		-		- -	-
Interface								
Interface reduction factor	R_{inter}	0,7	0,7	0,7	0,7	0,7	-	-

** obtained from Rødvand et al., 2019*
*** obtained from MulticonsultASA, 2017*

Table 3.6: Model parameters for jet grouting

Description			Unit
Unit weight	γ	25	kN/m^3
Poisson's ratio	υ'	0,15	-
Model parameters Mohr-Coulomb			
Drainage type	*Type*	Undrained (B)	-
Stiffness	*E'*	1,370E6	kPa
Undrained shear strength	$s_{u,ref}$	3170***	kPa
Model parameters Shotcrete			
Drainage type	*Type*	Non-Porous	
Young's modulus after 28 days	E_{28}	1,369E6	kPa
Uniaxial compressive strength after 28 days	$f_{c,28}$	5121	kPa
Uniaxial tensile strength after 28 days	$f_{t,28}$	50**	kPa
Normalized initial yield stress in compression	f_{c0n}	0,21*	
Normalized failure strength	f_{cfn}	0,1*	
Normalized residual strength	f_{cun}	0,1*	
Plastic peak strain in uniaxial compression at age 1h, 8h and 24 h	ε_{cp}^p	-0,006	
Increase ε_{cp}^p with p	a	16*	
Fracture energy in compression after 28 d	$G_{c,28}$	0,07189	kPa
Normalized residual tensile strength	f_{tun}	0	

** From PLAXIS Manual*
*** IS456:2000, 2000*
**** from UCS by Keller*

Table 3.7: Model parameters for anchors

Layers		Top anchor	Bottom anchor	Unit
Material model	*Model*	Elastic	Elastic	-
Anchor Stiffness	EA	358 200	689 400	kN
Planar Spacing	$L_{spacing}$	2,7	2,7	m

3.4.3 Construction Phases

Table 3.8 tabulates the construction phases implemented in the model. Gravity loading is implemented for the initial phase to ensure that the initial stresses in the model is correct. Due to the sloping bedrock depth, using K_0-procedure as the initial phase would lead to an incorrect initial stress states (Gouw, 2014). Dry excavation was conducted in the study site, thus at every excavation stage, the excavated cluster is set to dry.

Table 3.8: Construction stages

Phase	Construction stage	Type	Note
Initial Phase	Initial Phase	Gravity Loading	-
1	Construction of jet grout retaining wall	Plastic	-
2	Construction of KC columns	Plastic	-
3	Excavation to GL -3 m	Plastic	-
4	Installation top anchors at GL -2 m	Plastic	Pre-stressed at 293 kN
5	Excavated to GL -5 m	Plastic	-
6	Installation bottom anchors at GL -4.5 m	Plastic	Pre-stressed at 586 kN
7	Excavated to GL -6 m	Plastic	-

3.4.4 Mesh Sensitivity Study

Prior to final analysis of the model, a mesh sensitivity study is conducted to ensure that mesh settings do not affect the final model outputs.

The mesh study is conducted by using 5 different mesh refinements on the model where jet grouts are modelled using Shotcrete model. This is because the model predicts strain softening post-yielding. This may cause problems as strain softening behaviour often exhibits mesh dependency. Table 3.9 below tabulates the results of the mesh sensitivity study.

Table 3.9: Mesh sensitivity study results

Mesh Sensitivity Study	
Mesh Refinement Setting	**Total Displacement |u| (mm) in Last Phase**
Very Coarse	N.A.
Coarse	13,2
Medium	12,3
Fine	12,0
Very Fine	11,9

The study have shown that the model is slightly affected by the mesh refinement setting where the observed final total displacement is decreasing as the mesh settings become finer. Nevertheless, the study concludes that in overall, the model is considered to be insensitive since the difference in the total displacement between the mesh settings is negligible especially after "Medium" refinement.

It is noted that using "Very Coarse" refinement, the model is unable to achieve equilibrium in the initial phase. One hypothesis to explain this phenomena is the formation of ill-conditioned elements. In PLAXIS, the individual elements have triangular shapes. As the elements get larger, the nodes are more likely to experience difference stress states. This may cause excessive deformation in one of the nodes, causing the elements to be elongated, making it difficult to achieve global equilibrium.

3.4.5 Interface Sensitivity Analysis

Interfaces are introduced for the contact between the soil and the jet grout columns. A sensitivity analysis was conducted to identify the impact the interfaces have on the models.

The result of the sensitivity analysis are presented in table 3.10. In the model the interface have a small impact on the simulated movements, up to 0,5 mm for wall deflection and 0,4 mm for settlements. This is in line with the expectations that the interface strength factors should not affect the outcome of the analysis.

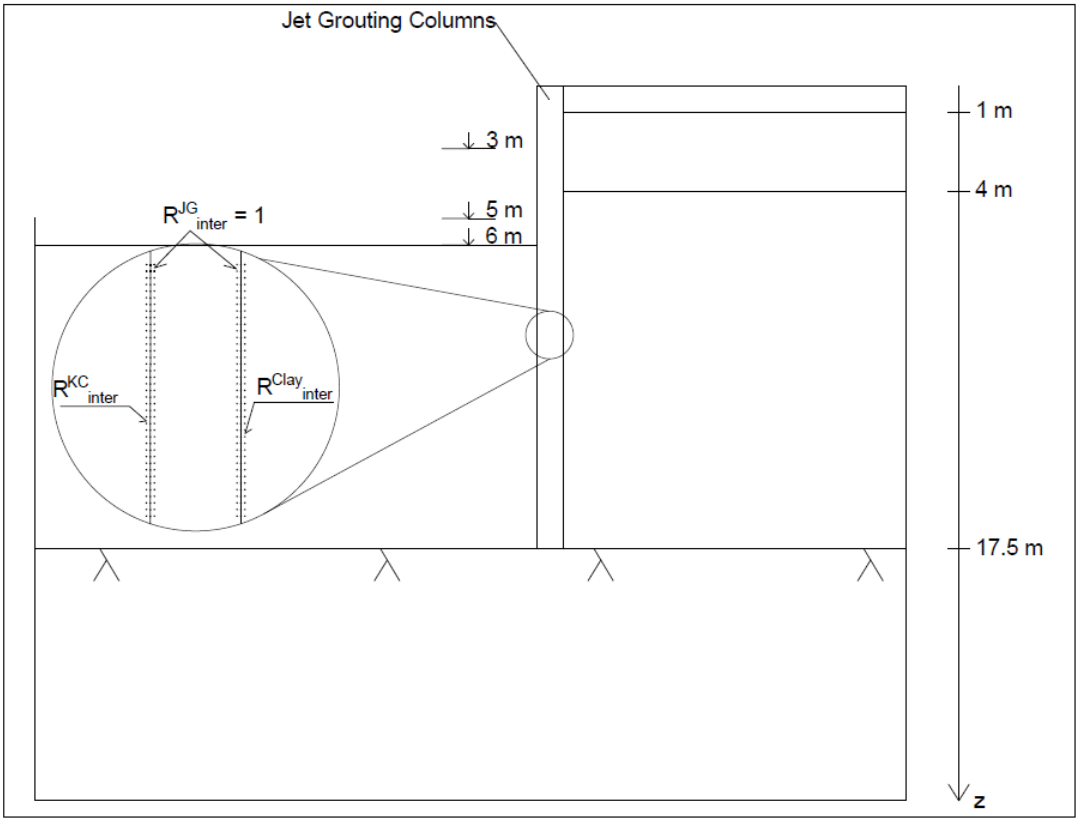

Figure 3.19: Image of the the interface value around the modelled jet grouted retaining wall

Table 3.10: Interface setting sensitivity analysis study results

R_{inter}^{Clay}	R_{inter}^{KC}	Max wall deflection (mm)	Settlements (mm)
0,7	0,8	10,8	3,2
0,6	0,7	11,0	3,3
0,5	0,6	11,1	3,3
0,4	0,5	11,3	3,4

4

Results & Discussions

This chapter will explore the suitability of the Shotcrete material model. This is done by comparing the results of the simulations from both the Shotcrete and MC models. Similarities and/or differences observed in the results will then be explained when possible. A model validation is then performed, where the simulation results are compared to actual readings monitored on site. The practicality aspect of Shotcrete material model will also be discussed.

Lastly, limitations introduced in the earlier chapter will be discussed on how they affect the outcome of the simulations.

4.1 Suitability of Shotcrete Material Model

4.1.1 Model Comparison

In this thesis, two deformation analysis at the last phase were conducted and they are: i) the jet grout column horizontal displacement; and ii) the ground surface settlement on the active side of the excavation. Figure 4.1 below illustrates these displacement distribution, whereas Figure 4.2 shows the build-up of the column vertical displacement.

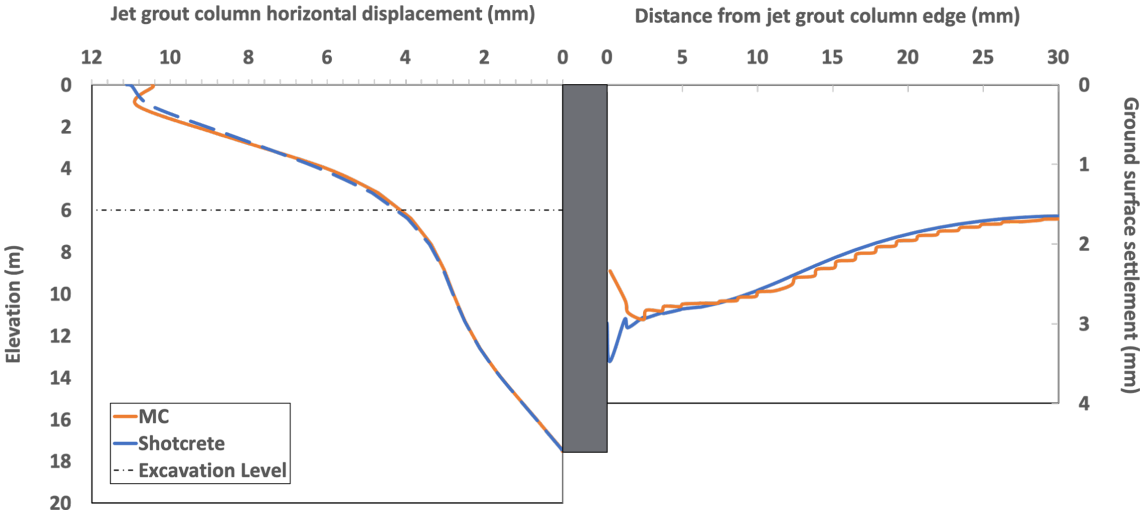

Figure 4.1: Displacement plot surrounding jet grouting columns

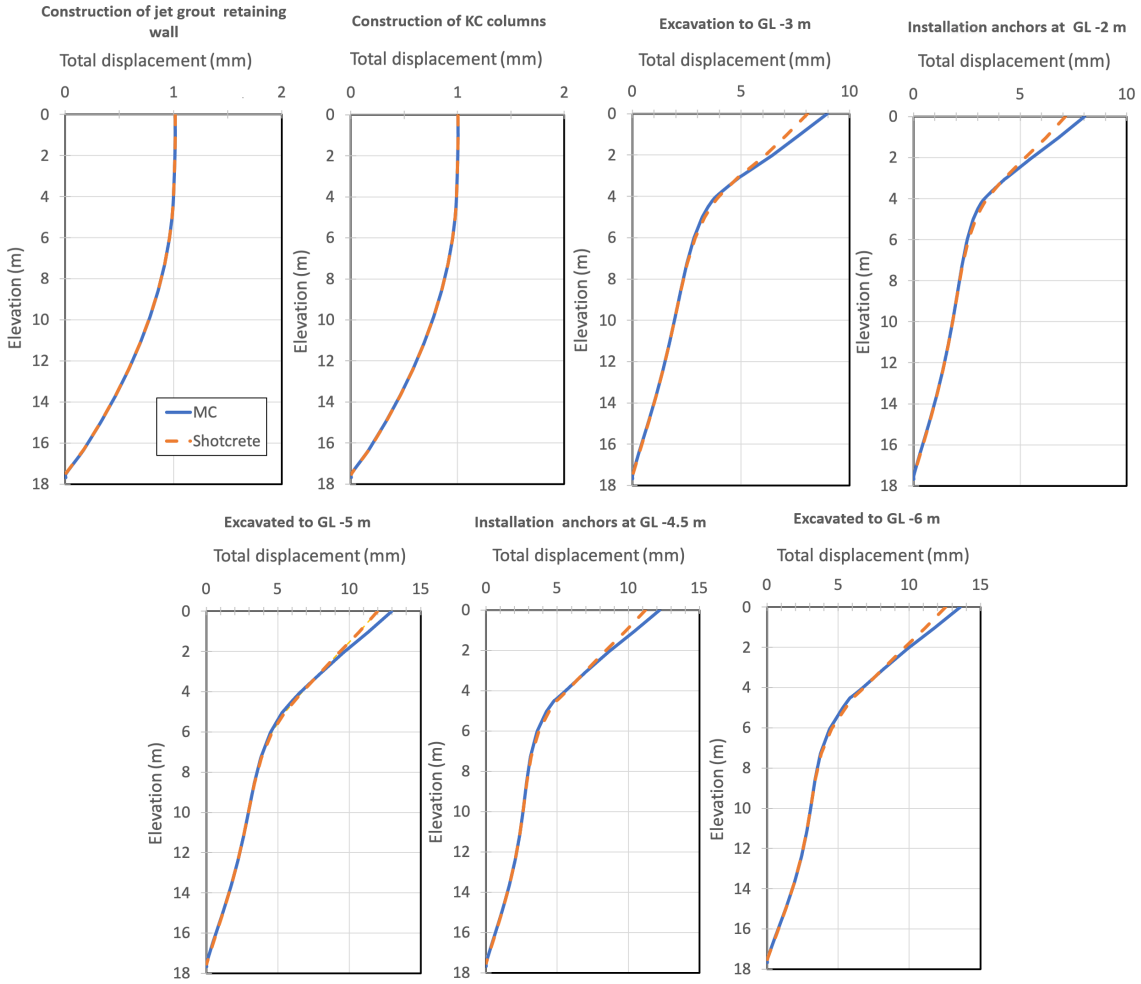

Figure 4.2: Plot of the total displacement in different phases

It is observed that displacement predicted by the two models are largely similar to each other and is within the acceptable level as defined in the previous chapter. The maximum horizontal displacement predicted by the two models are similar (11,1mm in Shotcrete vs 10,8mm in MC) although the location where it takes place is slightly different. In the MC model, maximum horizontal displacement takes place on the surface, whereas that in the Shotcrete model occurs approximately 1m below the surface.

Similar observation can be seen for the ground surface settlement. The maximum settlement predicted by the MC model is 2,95mm, whereas that predicted by the Shotcrete model is 3,48mm.

One hypothesis that can explain the similarity is that in both models, the jet grout material is still within the elastic region. As explained in the previous chapter, the novelty of the Shotcrete material model lies in the post-yielding region. Otherwise, the model adopts a Mohr-Coulomb failure criterion as the yield surface, which is the same as the MC model. Therefore, the differences between the two material models

are only prominent in the post-yielding region when the material is near failure. This observation is in-line with another similar previous study of the Shotcrete model on deep soil mixing wall (Waichita et al., 2020).

Furthermore, the displacement of the jet grout column is largely controlled by the system. In this study site, soil makes the majority of the system. As they are identical in both models, the magnitude of the displacement is expected to be the same as well. This can be observed in Figure 4.3 where the earth pressures, both active and passive, are identical in both models. Additionally, the presence of the anchors may also affect the displacement.

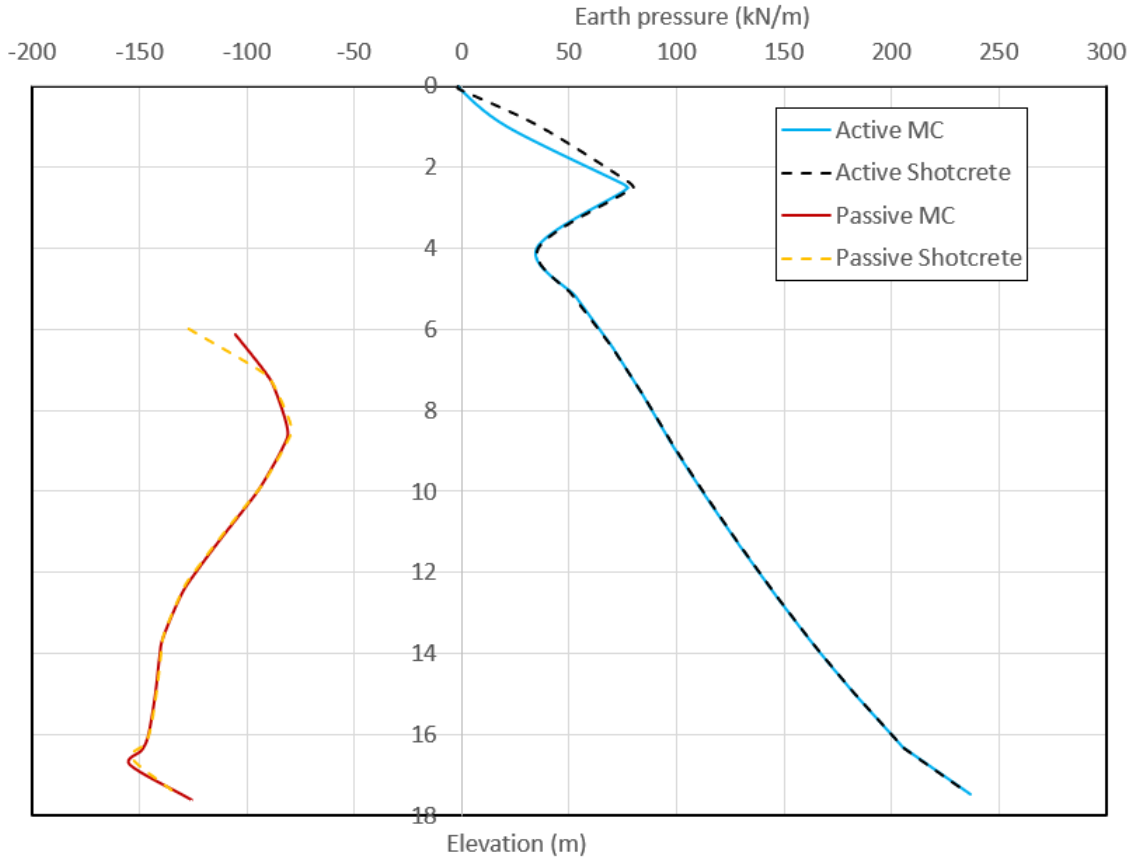

Figure 4.3: Plot of the earth pressure acting on the jet grouting columns

4.1.2 Practicality of Shotcrete Material Model

Since jet grout material has been commonly modelled using the MC material model, there is no issue in determining its model parameters. However, the opposite is true for Shotcrete model. Table 4.1 tabulates the source of model parameters that are unique to the Shotcrete model in this study.

Table 4.1: Source of Model Parameters Specifically for Shotcrete Material Model

Model Parameters	Source		
	Original Tests	**Additional Tests**	**Literature or PLAXIS Manual**
E_{28}	✓		
$f_{c,28}$	✓		
$f_{t,28}$			✓
f_{c0n}			✓
f_{cfn}			✓
f_{cun}			✓
ε^p_{cp}	✓		
a			✓
$G_{c/t,28}$		✓	
f_{tun}			✓

In the original geotechnical investigation, only UCS tests were conducted for the jet grout material. With the results, only 3 model parameters were able to be determined. Considering that tests that are commonly conducted in the industry are UCS and uniaxial tensile tests, the common tests would then be able to determine only 4 model parameters, E_{28}, $f_{c,28}$, $f_{t,28}$ and ε^p_{cp}.

The fracture energy $G_{c/t,28}$ were determined through WSTs conducted for the purpose of the thesis. They were chosen because the model is known to be sensitive to these parameters (Waichita et al., 2020). However, these tests are not commonly conducted in the industry. Furthermore, as mentioned in the previous chapter, WST samples were collected from the spoil instead of cored. Spoil contains impurities and thus does not accurately represent the jet grout material. However, there are difficulties in obtaining cored cube samples that have wedges for the purpose of the test.

The other parameters, which are f_{c0n}, f_{cfn}, f_{cun}, a and f_{tun}, were directly obtained from the PLAXIS manual (PLAXIS, 2019). Nevertheless, the parameters recommended in the manual is only for either cured or sprayed concrete (PLAXIS, 2019). It is unknown if the same set of values can be used for jet grout material. Furthermore, these model parameters are not easily determined and require further research.

4.1.3 Comparison Analysis

In short, the findings of this study thus far is:

- Simulation using the Shotcrete model produced results that are similar to that using the MC model since the material did not leave the elastic region.

- Tests that are commonly conducted in the industry can only provide 4 (out of 10) model parameters that are unique for the Shotcrete model. Additional tests were conducted in this study to determine another parameter, but the other 5 parameters were determined using values from PLAXIS Manual. These values were not meant for jet grout material, and further research will be required to

identify whether these values can actually be used for jet grout material.

Based on the aforesaid findings, this study has concluded that, for this site specifically, it is unnecessary to adopt Shotcrete material model to replace the MC material model for jet grouting deformation analysis. In the industry, earth retaining structures are designed to minimise movements, which is critical to avoid catastrophic failure. This is especially true in urban settings such as the study site used in this thesis, where there are existing buildings in the vicinity and thus need to protected from not only excessive settlement, but also differential settlement. This means that the serviceability limit state (SLS) is governing than the ultimate limit state (ULS). As a result, in terms of ULS, the structure is over-designed. Hence, the material is unlikely to be in the post-yielding region where the Shotcrete model excels. Coupled with the fact that further tests and research need to be conducted to accurately obtain model parameters for jet grout materials, there is not enough merit to pursue using Shotcrete model over MC model.

4.2 Discussion on Limitations

Several assumptions for this study can affect the accuracy of the model predictions. As can be seen in the site layout, the site is not symmetrical. Additionally, the section where jet grout columns are installed are located near a corner. Hence, plane strain analysis assumed for this study is not accurate, which may affect the accuracy of the prediction.

Soil profile is assumed on the active side of the study site since boreholes were only available in the passive side. Since the active side is the area generating the most load on the jet grout columns, it is important to ensure that the soil profile here is modelled accurately. Furthermore, the existing buildings are assumed to not affect the excavation side. This is because the buildings are assumed to be founded on piles. However, if the foundation is not on piles, these buildings can affect the accuracy of the model.

Notwithstanding the above-mentioned implications of the assumptions, the focus of this study is to analyse and compare the deformations of the jet grout columns between the two models. As such, as long as the load on the columns are identical in the two models as seen in Figure 4.3, the comparison will remain accurate.

Another feature of the Shotcrete material model is its ability to model the time-dependency of the strength and stiffness properties of the jet grout material. This means that the model is able to predict the behaviour of the material from the moment it is cast up to 28 days, after which the properties are no longer time-dependent. The reason why those parameters are not explored in this study is because in the industry, the columns will only be loaded once the jet grout material has cured to gain sufficient strength. As such, it is unnecessary to include the time-dependency factor into the model since it will not be utilised.

5

Conclusions & Recommendations

This thesis has analysed the suitability of Shotcrete material model for jet grout deformation analysis in PLAXIS. This was done by creating two identical simplified models based on an actual excavation site located in Oslo, Norway. One of them used Shotcrete to model the jet grout columns, while the other is based on Mohr-Coulomb model, one that is commonly used in the industry. The summary of this thesis is:

- A simplified model of the study site is created using the assumption of plane strain analysis and plane symmetry. Model parameters required for the model system is obtained via provided data from the original geotechnical investigation conducted for the purpose of the actual project. If the data is insufficient, literature values from the vicinity are used.

- Additional tests in the form of wedge splitting tests (WSTs) were conducted to determine the fracture energy of the jet grout material.

- Lime-cement (KC) columns were installed in the excavation site. However, coverage was only partial. To accurately model the effect the columns, a KC-clay composite material was proposed where the model parameters are derived from the percentage content of KC and soft clay for a given volume of space.

- Data obtained from the original geotechnical investigation are insufficient to complete the model parameters required for the Shotcrete model. While WSTs were conducted to supplement the original data, several model parameters require further research to determine the correct values for jet grout material.

- Simulation results of the two models have shown that the predicted deformations are virtually identical. This observation can be attributed to two reasons. The first is that, in reality, as opposed to the analyses carried out in industry, SLS is governing the response. This means that the material is over-designed in terms of failure, and will thus remain in the elastic region. Shotcrete model models the elastic region using Mohr-Coulomb failure criterion, which is similar to the Mohr-Coulomb model. Secondly, the deformation in the system is largely controlled by the entirety of the system. In this case, the model contains not only the soil, which makes the majority of the system, and the jet grout retaining wall, but also the presence of anchors. The system, with the exception of the jet grout material, is modelled similarly in the two models,

which may result in the little to no difference in the deformations.

- While the Shotcrete model is able to model time-dependency stiffness and strength properties of the material, this feature was not explored in this study. The reason is because on site, the columns are left to cure prior to any excavation work.

Based on the summary above, the following recommendations for further research is provided:

- Further research on the comparison between the two models where the jet grout columns are loaded until yield would be recommended. As it is unsafe to do so in actual excavation site, a 1-g or centrifuge physical model of the study site is suggested. In the model, excavation can be continued, thus increasing the lateral load on the columns.

- Further research to determine accurate model parameters specifically for the Shotcrete model. In particular, usage of the normalised initial yield stress, failure strength and residual strength in this study based on the PLAXIS manual can be further explored.

Bibliography

Bredy, S., Jandora, J. et al. (2019). Three-dimensions modelling of a jet pile construction in the karolinka dam. *Acta Universitatis Agriculturae et Silviculturae Mendelianae Brunensis*, *67*(3), 637–648.

Brühwiler, E., & Wittmann, F. (1990). The wedge splitting test, a new method of performing stable fracture mechanics tests. *Engineering fracture mechanics*, *35*(1-3), 117–125.

Clough, G. W. (1990). Construction induced movements of in situ walls. *Design and performance of earth retaining structures*, 439–470.

Craig, R. F. (2004). *Craig's soil mechanics*. CRC press.

Croce, P., Flora, A., & Modoni, G. (2014). *Jet grouting: Technology, design and control*. Taylor & Francis. https://books.google.se/books?id=E53AAgAAQBAJ

Duncan, J. M., & Chang, C.-Y. (1970). Nonlinear analysis of stress and strain in soils. *Journal of Soil Mechanics & Foundations Div*.

Eide, O., Aas, G., & Josang, T. (1972). Special application of cast-in-place walls for tunnels in soft clay in oslo. *Fifth Eur Conf On Soil Proc/Sp/*, (Conf Paper).

Feng, H. (2009). Plaxis finite elements analysis on supporting structure with high-pressure jet grouting pile and composite soil-nailing wall [j]. *Exploration Engineering (Rock & Soil Drilling and Tunneling)*, *9*.

Gouw, T.-L. (2014). Common mistakes on the application of plaxis 2d in analyzing excavation problems. *International Journal of Applied Engineering Research*, *9*(21), 8291–8311.

Ignat, R., Baker, S., Karstunen, M., Liedberg, S., & Larsson, S. (2020). Numerical analyses of an experimental excavation supported by panels of lime-cement columns. *Computers and geotechnics*, *118*, 103296.

IS456:2000. (2000). Is456:2000 code of practice for plain and reinforced concrete (fourth edition.

Karstunen, M., & Amavasai, A. (2017). Best soil: Soft soil modelling and parameter determination.

Keller. (2021). Private photo sent by keller.

Kupfer, H. B., & Gerstle, K. H. (1973). Behavior of concrete under biaxial stresses. *Journal of the engineering mechanics division*, *99*(4), 853–866.

Lambe, T. W., & Whitman, R. V. (1969). Soil mechanics.

Lazarte, C. A., Robinson, H., Gómez, J. E., Baxter, A., Cadden, A., & Berg, R. (2015). *Soil nail walls reference manual* (tech. rep.).

Long, M. (2001). Database for retaining wall and ground movements due to deep excavations. *Journal of Geotechnical and Geoenvironmental Engineering*, *127*(3), 203–224.

Lunne, T., Berre, T., & Strandvik, S. (1997). Sample disturbance effects in soft low plastic norwegian clay. *Symposium on Recent Developments in Soil and Pavement MechanicsCAPES-Fundacao Coordenacao do Aperfeicoamento de Pessoal de Nivel Superior; CNPq-Conselho Nacional de Desenvolvimento Cientifico a Tecnologico; FAPERJ-Fundacao de Ampora a Pesquisa do Estado do Rio de Janeiro; FINEP-Financiadora de Estudos e Projetos*.

Maatkamp, T., Gavin, K., Brinkgreeve, R., Everts, H., Loonen, N., & Lagendijk, P. (2016). *The capabilities of the plaxis shotcrete material model for designing laterally loaded reinforced concrete structures in the subsurface*.

Modoni, G., & Bzówka, J. (2012). Analysis of foundations reinforced with jet grouting. *Journal of Geotechnical and Geoenvironmental Engineering*, *138*(12), 1442–1454.

Modoni, G., Croce, P., & Mongiovi, L. (2006). Theoretical modelling of jet grouting. *Géotechnique*, *56*(5), 335–347.

MulticonsultASA. (2017). 28517-1-rig-not-006a-rev01 beregningsnotat plaxis-input kværnerdammen, f1 1.

Nakanishi, W. (1974). Method for forming an underground wall comprising a plurality of columns in the earth and soil formation [US Patent 3,800,544].

Norconsult. (2019). Geoteknisk prosjekteringsrapport.nytt klinikk- og protonbygg radiumhospitalet.

Ochmański, M., Modoni, G., & Bzówka, J. (2015). Prediction of the diameter of jet grouting columns with artificial neural networks. *Soils and Foundations*, *55*(2), 425–436.

ORP. (2017). Geoteknisk datarapport.

PLAXIS. (2019). Plaxis material models manual 2019. *PLAXIS bv, the Netherlands*.

Reynolds, O. (1885). Lvii. on the dilatancy of media composed of rigid particles in contact. with experimental illustrations. *The London, Edinburgh, and Dublin Philosophical Magazine and Journal of Science*, *20*(127), 469–481.

Rødvand, L., Andresen, L., & Grimstad, G. (2019). Case study of a road bridge hit by a landslide in highly sensitive clay. *Proceedings of the XVII ECSMGE*.

Roscoe, K., & Burland, J. (1968). On the generalized stress-strain behaviour of wet clay.

Saurer, E., Marcher, T., Schädlich, B., & Schweiger, H. (2014). Validation of a novel constitutive model for shotcrete using data from an executed tunnel/validierung eines neuen stoffgesetzes für spritzbeton mittels ergebnissen eines ausgeführten tunnelprojekts. *Geomechanics and Tunnelling*, *7*(4), 353–361.

Schädlich, B., & Schweiger, H. (2014). A new constitutive model for shotcrete. *Numerical methods in geotechnical engineering*, *1*, 103–108.

Schanz, T., Vermeer, P., & Bonnier, P. G. (2000). The hardening soil model: Formulation and verification. *Beyond*, *1999*, 281.

Schütz, R., Potts, D., & Zdravkovic, L. (2011). Advanced constitutive modelling of shotcrete: Model formulation and calibration. *Computers and Geotechnics*, *38*(6), 834–845.

Schweiger, H., Sedighi, P., Henke, S., & Borchert, K. (2014). Numerical modelling of ground improvement techniques considering tension softening. *Proc., 8th Int.*

Symp. on Geotechnical Aspects of Underground Construction in Soft Ground, Korean Geotechnical Society, Seoul, South Korea, 209–214.

Terzaghi, K., Peck, R. B., & Mesri, G. (1996). *Soil mechanics in engineering practice*. John Wiley & Sons.

Toraldo, C., Modoni, G., Ochmański, M., & Croce, P. (2018). The characteristic strength of jet-grouted material. *Geotechnique*, *68*(3), 262–279.

Waichita, S., Jongpradist, P., & Schweiger, H. F. (2020). Numerical and experimental investigation of failure of a dcm-wall considering softening behaviour. *Computers and Geotechnics*, *119*, 103380.

Whittle, A., & Davies, R. (2006). Nicoll highway collapse: Evaluation of geotechnical factors affecting design of excavation support system. *International conference on deep excavations*, *28*, 30.

Zhang, W., Hong, L., Li, Y., Zhang, R., Goh, A. T., & Liu, H. (2021). Effects of jet grouting slabs on responses for deep braced excavations. *Underground Space*, *6*(2), 185–194. https://doi.org/10.1016/j.undsp.2020.02.002

A

Appendix

A.1 Calculation for Soft Soil Parameters

A.1.1 Calculation from triaxial tests

In this section the data and the calculation process for the triaxial test is presented.

A.1.1.1 Calculation to find elastic stiffness modulus

The calculation was done according to Section 3.3.7. Where $a = 0$, $p_{ref} = 100\ kPa$ and $m = 1$

$E'_{50} = E^{ref}_{50}(\frac{\sigma'_3+a}{p_{ref}+a})^m$

$E'_{50} = E_{50} * \frac{1}{3}$

Table A.1: Table of values from triaxial stress-strain graph

Parameter	Borehole 3	Borehole 8	Borehole 9
E_{50} (kPa)	12754	14266	13914
σ_3 (kPa)	62,6	58,1	62
E'_{50} (kPa)	4251	4755	4638
E^{ref}_{50} (kpa)	6791	8184	7480

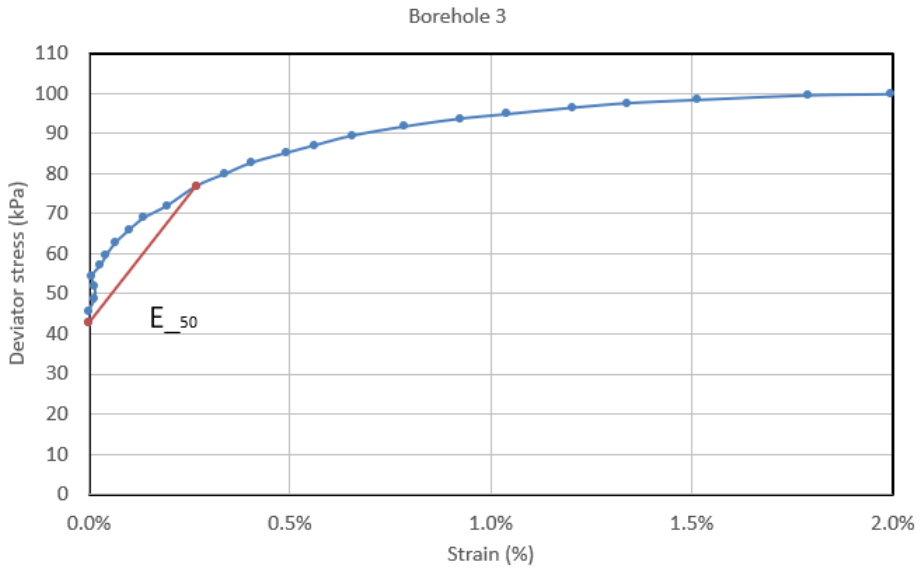

Figure A.1: Strain stress graph form triaxial test for borehole 3.

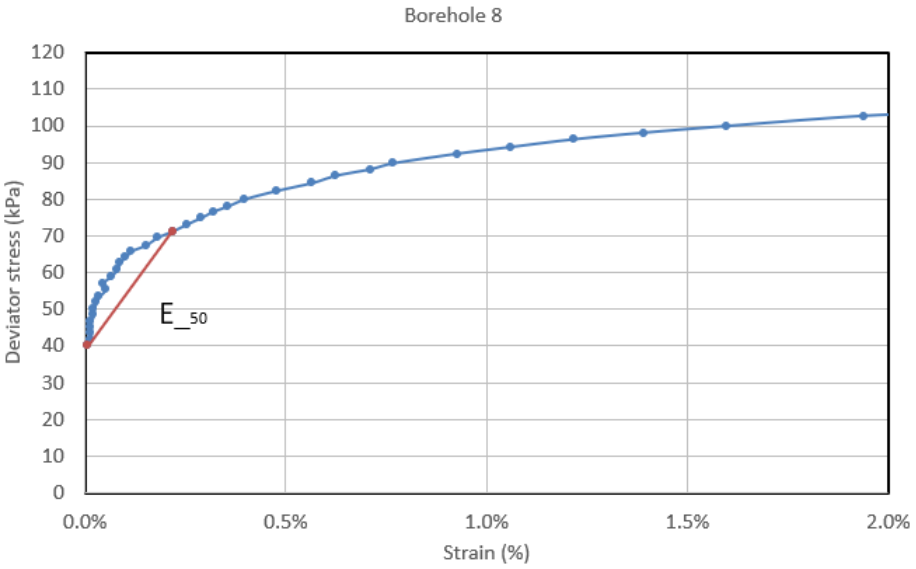

Figure A.2: Strain stress graph form triaxial test for borehole 8.

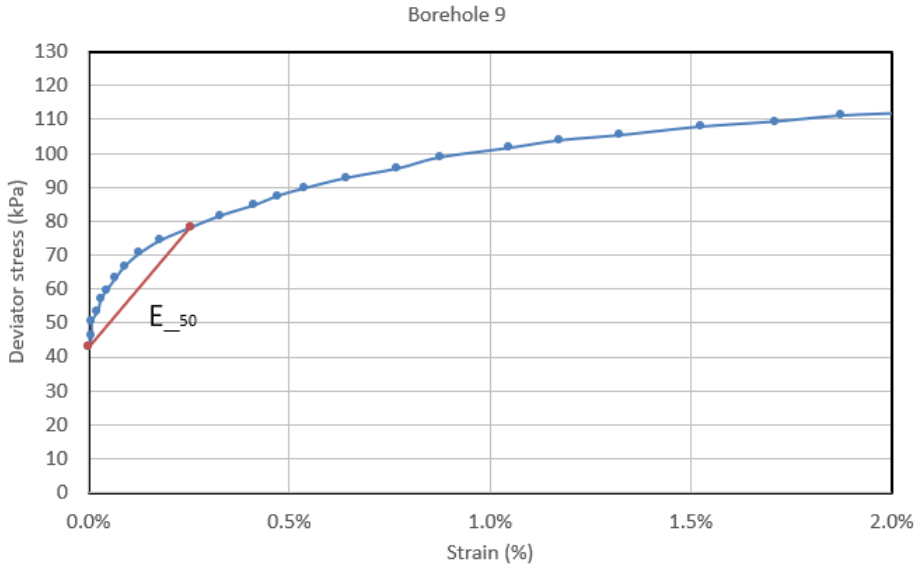

Figure A.3: Strain stress graph form triaxial test for borehole 9.

A.1.2 Calculation from oedometer CRS tests

In this section the data and the calculation process for the CRS test is presented.

A.1.2.1 Calculations for SS parameters

The soft soil parameters was found by taking the inclination of the lines. Also, the preconsolidation pressure was taken out from the CRS strain-stress data.

Table A.2: Input parameters for clay

Parameter	Notation	Borehole 3	Borehole 8	Borehole 9
Modified compression index	$\lambda*$	0,0527065	0,051764	0,051764
Modified swelling index	$\kappa*$	0,0059068	0,005068	0,005036
Pre consolidation pressure	p'_0	241	200	226
Over consolidation ratio	OCR	1,66	1,60	1,56

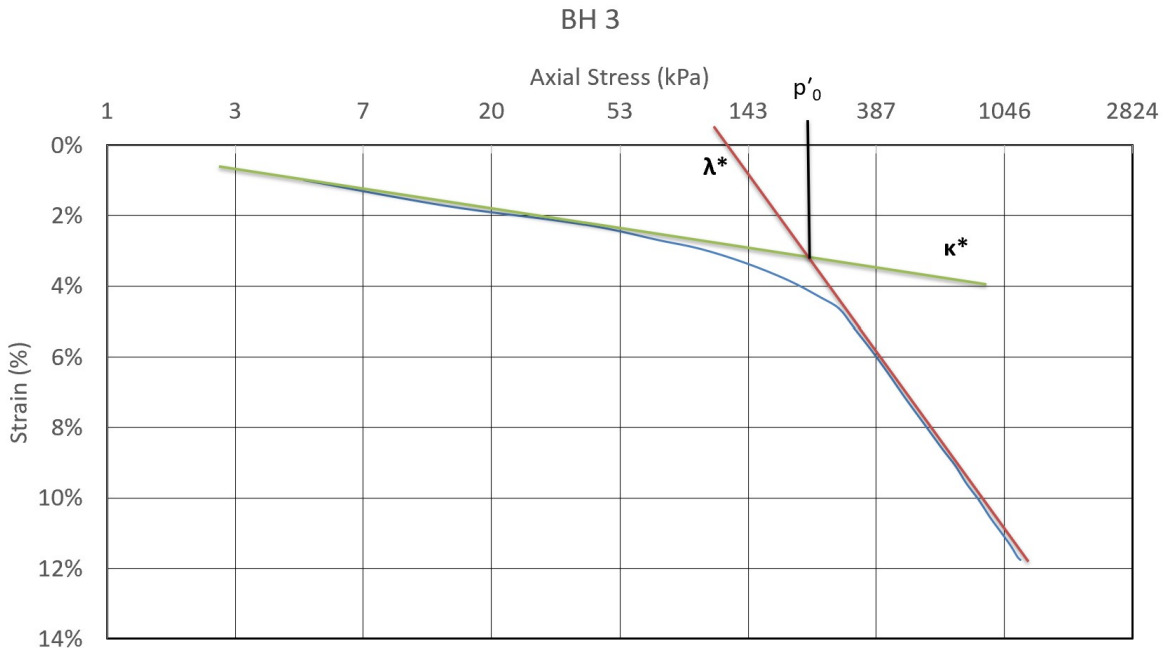

Figure A.4: Strain stress graph for borehole 3. Stress in ln-scale

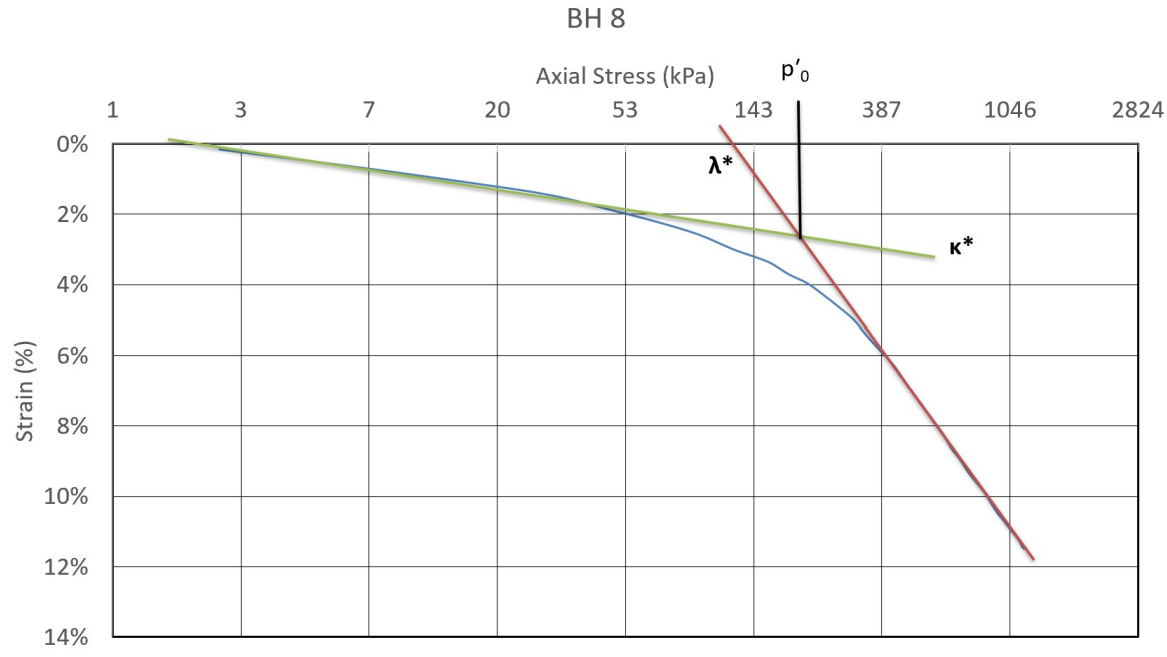

Figure A.5: Strain stress graph for borehole 8. Stress in ln-scale

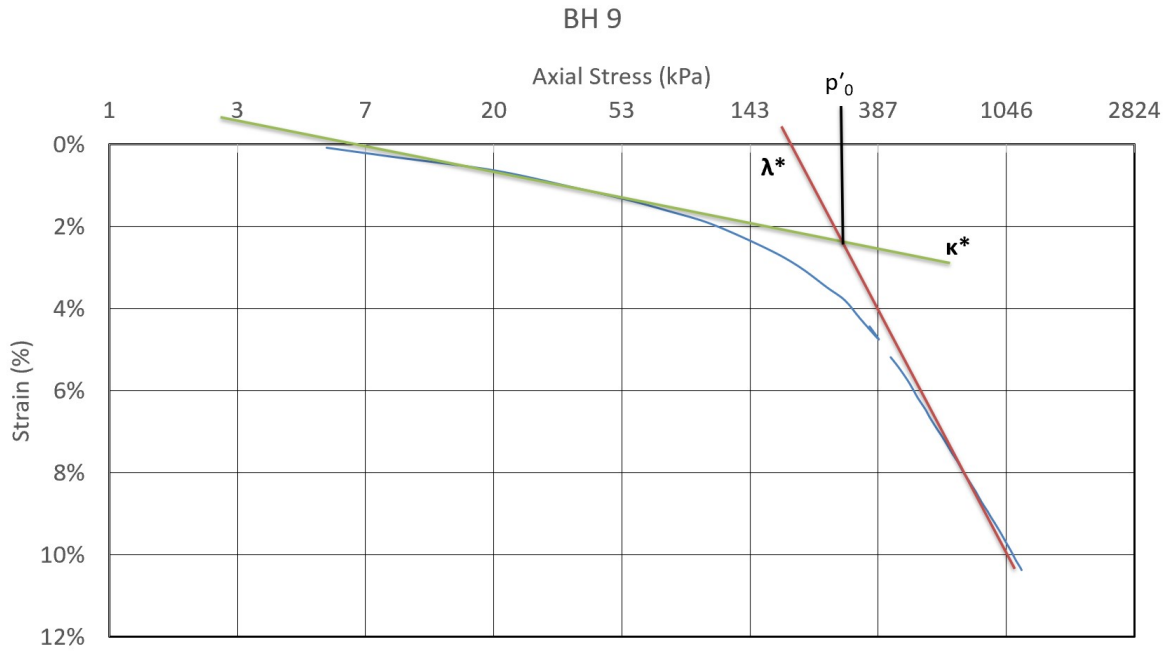

Figure A.6: Strain stress graph for borehole 9. Stress in ln-scale

A.1.2.2 CRS calculations for HS parameters

The calculation was done according to section 3.3.7. Where p_{ref} is 100 kPa. For borehole 9, σ_1 could not be identified and was not included in the calculations.

Table A.3: Calculation values for E_{oed}^{ref}

Parameter	Borehole 3	Borehole 8
E_{eod} (kPa)	17391	8823
σ_1 (kPa)	320	220
E_{oed}^{ref} (kPa)	5435	4010

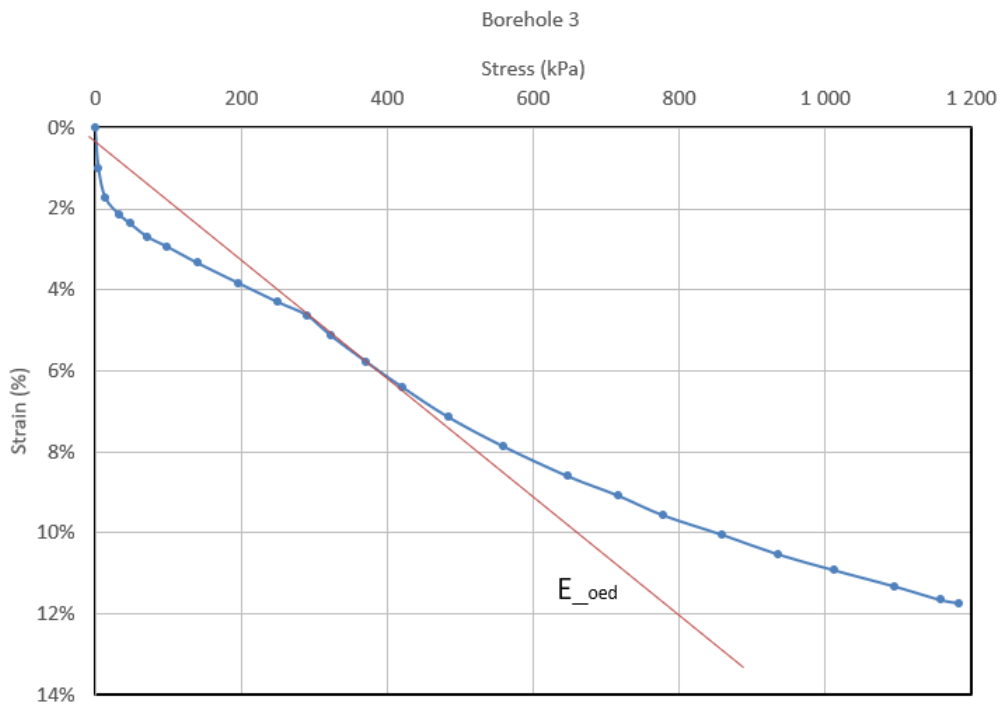

Figure A.7: Strain stress graph for borehole 3.

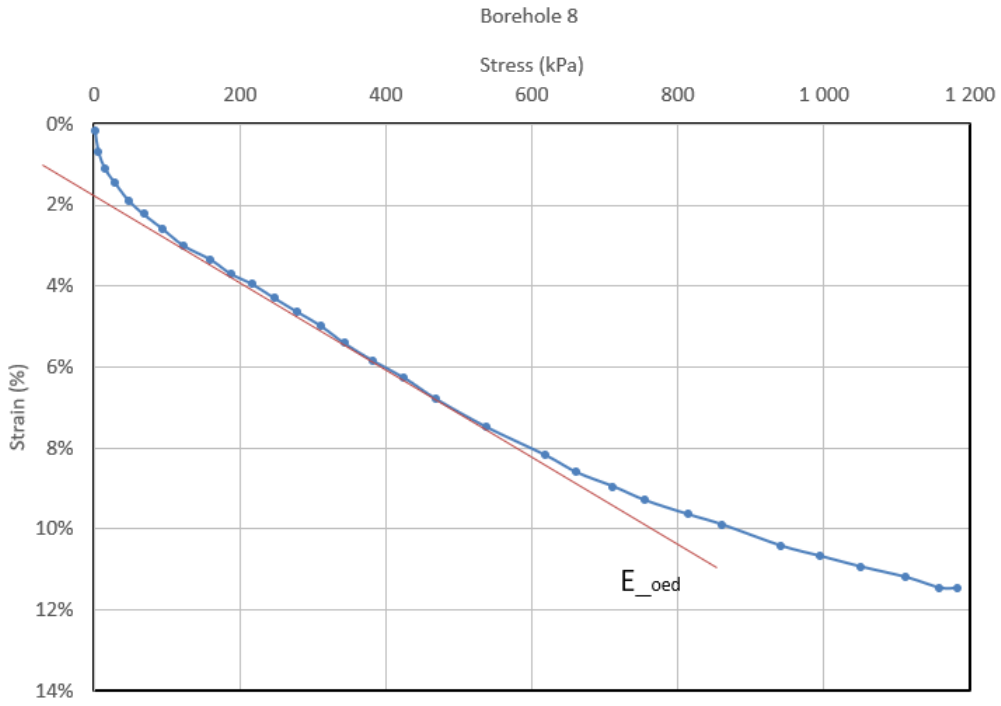

Figure A.8: Strain stress graph for borehole 8.

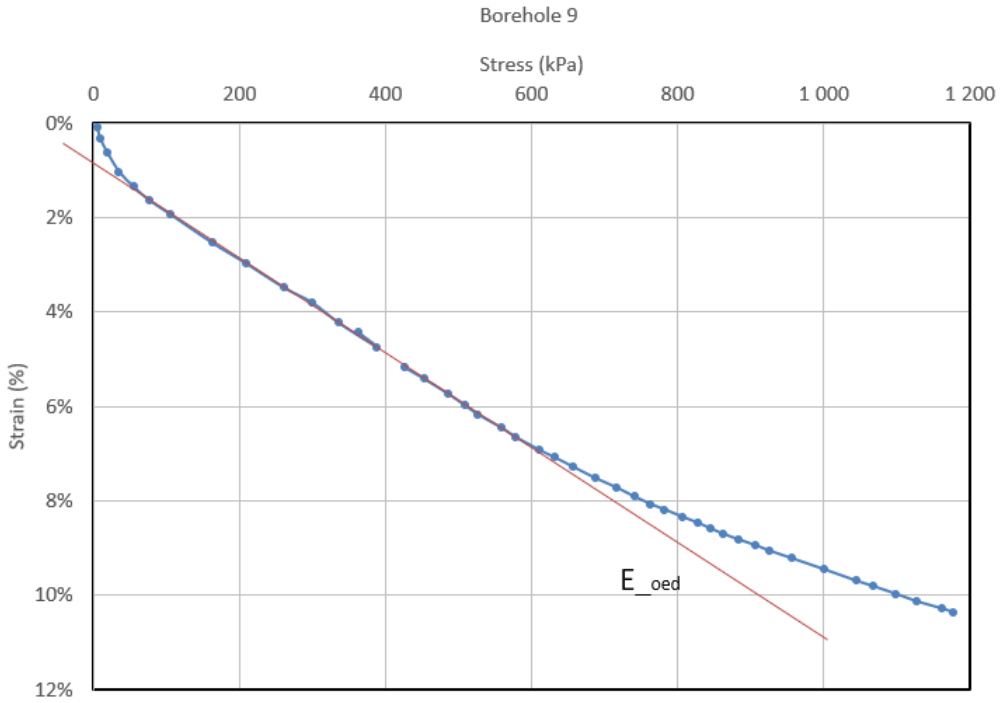

Figure A.9: Strain stress graph for borehole 9.

A.2 Calculations for Jet Grout Parameters

A.2.1 Calculations from UCS

The unconfined compressive strength was calculated by taking the average value from UCS 2, 3 and 4. After curing, UCS 1 already had some small fractures and was excluded from the results.

Table A.4: The input data from UCS results

Parameter		UCS 2	UCS 3	UCS 4
f_c (kPa)	Compressive strength	4,9	5,16	5,16
f_{c0n}	Normalised failure strength	0,22	0,21	0,21

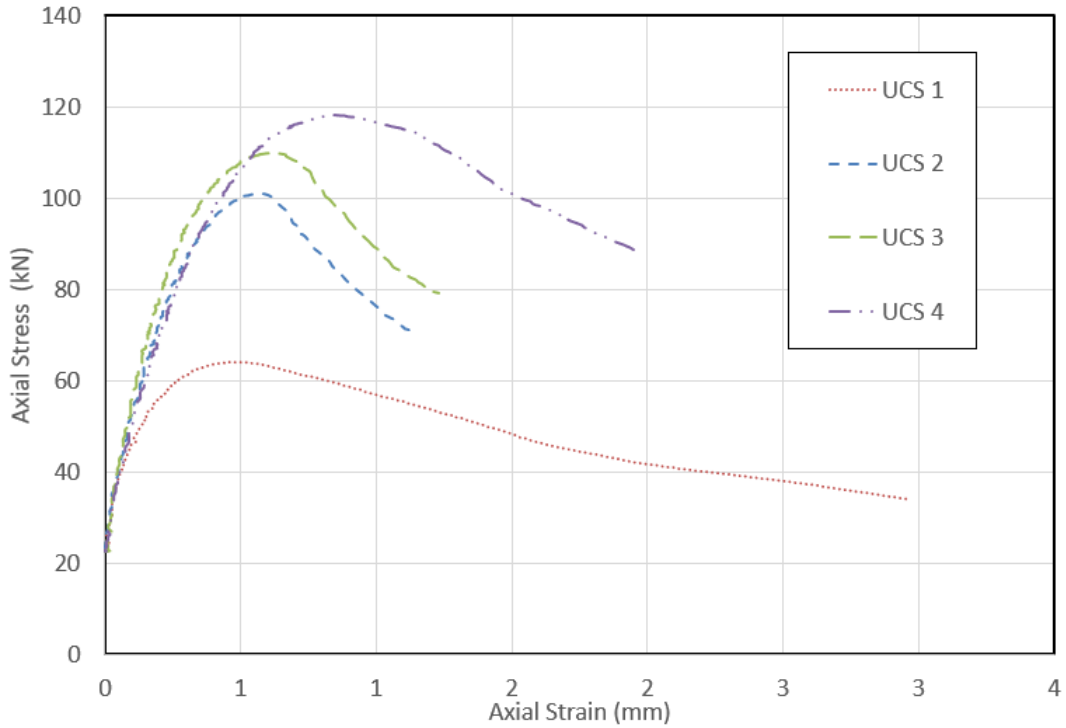

Figure A.10: UCS results

A.2.2 Calculations from WST

The specific fracture energy G can be calculated by taking the total fracture energy W divided by the fracture area. The total fracture energy is the area under the curve.
$G = W * A_f$

Table A.5: Results of WST

Parameter		WST 1	WST 2	WST 3
W (kNmm)	Fracture energy	0,810	0,746	0,753
A_F (m^2)	Fracture area	0,110	0,107	0,010
G (kN/m)	Specific fracture energy	0,074	0,070	0,072

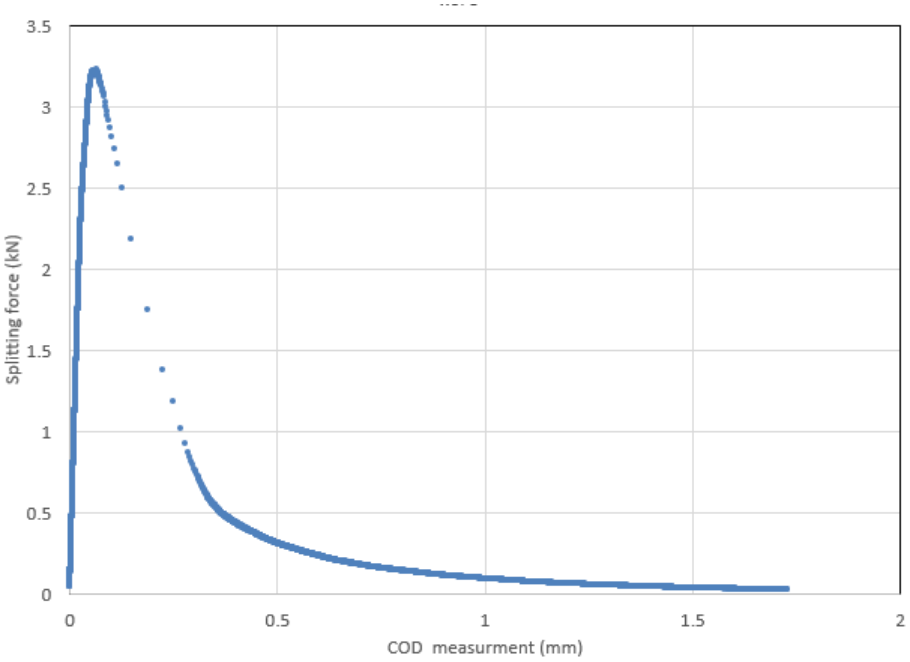

Figure A.11: Results from WST 1

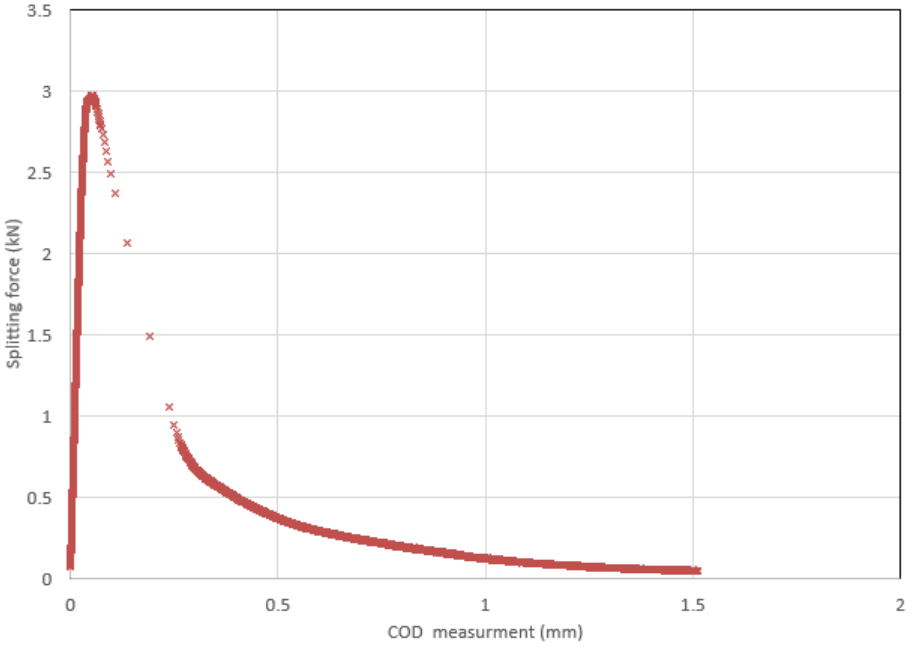

Figure A.12: Results from WST 2

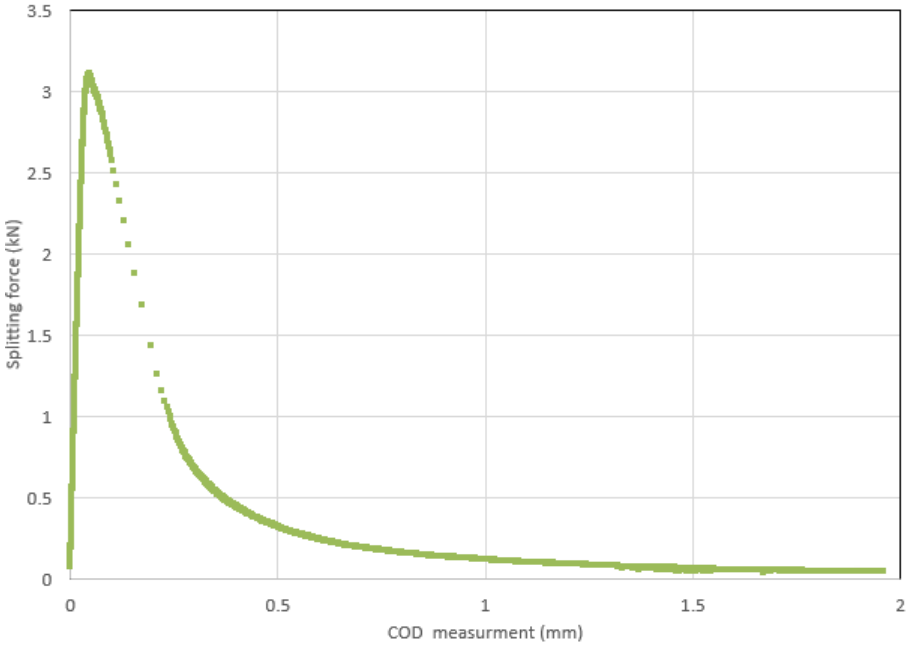

Figure A.13: Results from WST 3

A.3 Calculations for KC-clay Composite Parameters

The composite material is done with hardening soil. The remaining hardening soil parameters for clay are calculated. Then, the hardening soil parameters for KC is calculated. The parameters of the composite material is calculated by following equation.

$$Composite\ parameter = Clay\ parameter * clay\ \% + LC\ parameter * LC\ \%$$

The oedometric stiffness is calculated according to Plaxis manual. λ^* was calculated in previous section and $p^{ref} = 100kPa$.

$$E_{oed}^{ref} = \frac{p^{ref}\lambda^*}{=} 2400kPa$$

The hardening soil parameter for KC was calculated according to Ignat et al., 2020. From the undrained shear strength, the stiffness for hardening soil was calculated.

$$s_u = 100kPa$$

$$E_{50}^{ref} = 1120 * s_u = 112000kPa$$

$$E_{oed}^{ref} = E_{50}^{ref} = 112000kPa$$

$$E_{ur}^{ref} = E_{oed}^{ref} * 3 = 339000kPa$$

Table A.6: The calculation for the ratios of the composite material

	Clay	KC	Clay 30%	KC 70%	KC c/c 750	Clay 63%	KC 37%	KC c/c 1500
E_{50}^{ref}	7485	112 000	2245	78 400	80 645	4715	41 440	46 155
E_{oed}^{ref}	2400	112 000	720	78 400	79 120	1512	41 440	42 952
E_{ur}^{ref}	35 000	339 000	10 500	237 300	247 800	22 050	125 430	147 480

A.4 Anchors

In the model the anchors was linear elastic. The input parameters are Young's modulus and cross-section area. Young's modulus was chosen according to Euro-code 3 where the $E = 210GPa$. The area was calculated according to the equation below. An appropriate steel class was chosen.

$Fd = 0,65 * fu * Area$

Steel class 355 $=>$ $f_u = 510MPa$

$Fd_{top} = 508kN => Area_{top} = 0,166cm^2$

$Fd_{bottom} = 1016kN => Area_{bottom} = 0,332cm^2$

DEPARTMENT OF SOME SUBJECT OR TECHNOLOGY
CHALMERS UNIVERSITY OF TECHNOLOGY
Gothenburg, Sweden
www.chalmers.se

CHALMERS
UNIVERSITY OF TECHNOLOGY